Nucleic Acids Research, 2024, **52**, 10543–10562
https://doi.org/10.1093/nar/gkae716
Advance access publication date: 21 August 2024
Nucleic Acid Enzymes

RudS: bacterial desulfidase responsible for tRNA 4-thiouridine de-modification

Rapolas Jamontas[1], Audrius Laurynėnas[2], Deimantė Povilaitytė[1], Rolandas Meškys[1] and Agota Aučynaitė[1,*]

[1]Department of Molecular Microbiology and Biotechnology, Institute of Biochemistry, Life Sciences Center, Vilnius University, 10257 Vilnius, Lithuania
[2]Department of Bioanalysis, Institute of Biochemistry, Life Sciences Center, Vilnius University, 10257 Vilnius, Lithuania
[*]To whom correspondence should be addressed. Tel: +37 062082954; Email: agota.aucynaite@bchi.vu.lt

Abstract

In this study, we present an extensive analysis of a widespread group of bacterial tRNA de-modifying enzymes, dubbed RudS, which consist of a TudS desulfidase fused to a Domain of Unknown Function 1722 (DUF1722). RudS enzymes exhibit specific de-modification activity towards the 4-thiouridine modification (s4U) in tRNA molecules, as indicated by our experimental findings. The heterologous overexpression of RudS genes in *Escherichia coli* significantly reduces the tRNA 4-thiouridine content and diminishes UVA-induced growth delay, indicating the enzyme's role in regulating photosensitive tRNA s4U modification. Through a combination of protein modeling, docking studies, and molecular dynamics simulations, we have identified amino acid residues involved in catalysis and tRNA binding. Experimental validation through targeted mutagenesis confirms the TudS domain as the catalytic core of RudS, with the DUF1722 domain facilitating tRNA binding in the anticodon region. Our results suggest that RudS tRNA modification eraser proteins may play a role in regulating tRNA during prokaryotic stress responses.

Graphical abstract

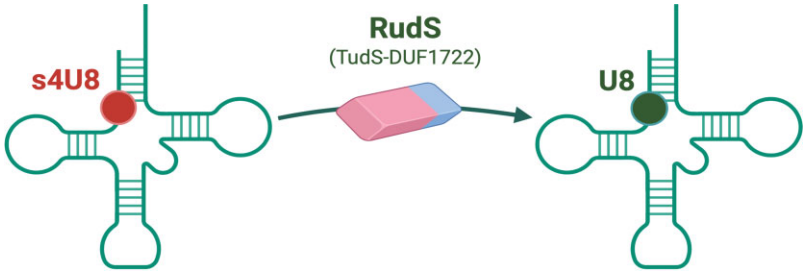

Introduction

Sulfur, an element pivotal for life, manifests its biological significance through diverse molecular forms, including the thiol groups of cysteines, thioethers of methionines, various cofactors (e.g., S-adenosyl methionine, Fe–S clusters), and as crucial post-transcriptional modifications in transfer RNAs (tRNAs) (1–4). The ubiquity of sulfur-containing tRNA modifications reflects their significance in cellular functions, affecting everything from codon recognition accuracy to thermal stability of tRNA molecules, pointing to their prospective roles in stress responses and cellular regulation (1,2,13–19,5–12).

One of the most abundant sulfur modifications in bacteria and archaea is 4-thiouridine (s4U), most commonly found at position 8 within a tRNA molecule (9,20). Some tRNA species, however, exhibit a second modification at position 9, resulting in two adjacent s4U modifications (21–23). ThiI, initially identified as an enzyme involved in thiamine biosynthesis in *Escherichia coli*, is typically regarded as the primary biosynthetic enzyme for s4U (24). In fact, enzymes responsible for s4U synthesis vary across species, exhibiting differing structural features and sulfur transfer mechanisms (9,25–28). Among sulfur-containing tRNA modifications, s4U stands out for its unique predispositions, including being a target for UV-A irradiation, which can impair translation by stalling the aminoacylation of cross-linked tRNAs (29,30). Moreover, the s4U modification contributes to the thermodynamical stability of tRNA molecules by significantly increasing their melting temperature (22,31) and affecting the efficiency of incorporation of other modifications (31,32).

Traditionally viewed as stable entities (33,34), bacterial tRNAs are now known to undergo rapid degradation under certain conditions, such as amino acid starvation (35), revealing a dynamic balance between tRNA synthesis and degradation (22). This balance is crucial for cellular adaptation to environmental stresses, where tRNA de-modifying enzymes could come into play with a regulatory role, modulating the tRNA pool in response to changing cellular conditions. Several de-modification/eraser enzymes, acting on individual modified

Received: May 13, 2024. **Revised:** July 30, 2024. **Editorial Decision:** August 1, 2024. **Accepted:** August 7, 2024

nucleosides or nucleobases have been described (36–43), as well as an enzyme that mediates subsequent C-to-U-to-Ψ conversion within tRNA (44). However, up to this date, the targeted removal of posttranscriptional modifications from tRNA was only reported for enzymatic demethylation in the context of eukaryotic tRNA homeostasis (45,46).

Despite extensive research into the biosynthesis of thio-modified nucleosides (2,9,47–52) the pathways for their enzymatic degradation remain less understood. The dual nature of sulfur, being indispensable yet potentially toxic, necessitates sophisticated cellular mechanisms for its safe storage and transfer. A growing body of evidence suggests that a class of sulfur transferases, including the TudS desulfidase, use a mechanism for direct sulfur transfer via Fe-S clusters (47–50,53–58). We recently provided experimental evidence that TudS enzymes, present in bacteria, archaea, and some eukaryotes, are desulfidases acting on thiolated bases, nucleosides, and their monophosphate and triphosphate derivatives with a preference for 4-thio-UMP (40). We also noted that TudS enzymes frequently have additional domains attached to them, potentially leading to a change in substrate preference that allows for the processing of larger molecules, including oligonucleotides or even the tRNA molecule.

Here, we report the discovery of RudS (tRNA 4-thiouridine desulfidases), a novel class of tRNA de-modifying/eraser enzymes. RudS are fusion proteins combining a TudS desulfidase domain and a domain of unknown function (DUF1722), which specifically target 4-thiouridine (s4U) modification in tRNA, demonstrating a direct role in the cellular management of sulfur-modified tRNAs. This paper explores the biochemical properties of RudS, elucidating its in vitro and in vivo activities. It also sheds light on the molecular interactions critical for its function, thereby contributing to our understanding of the complex regulatory networks governing tRNA stability and function in bacteria.

Materials and methods

Bacterial strains, plasmids and oligonucleotide primers

The bacterial strains used in this study are listed in Supplementary Table S1. The plasmid vectors used in this study are listed in Supplementary Table S2. The oligonucleotide primers used in this study are listed in Supplementary Table S3. Standard techniques were used for DNA manipulations (59). DNA primers were synthesized, and sequencing was performed by Azenta, Germany.

Construction of bacterial expression vectors

Bacterial vectors for expression in *E. coli* were constructed using the aLICator LIC Cloning and Expression Kit (Thermo Fisher Scientific, USA, #K1291). Bacterial genes were cloned directly from the genomic DNA and the viral gene was synthesized (Thermo Fisher Scientific, USA). The species and genes used in this study are listed in Table 1. Genes were cloned into pLATE11 and pLATE52 expression vectors as described in the manufacturer's protocol. Genomic DNA was isolated using Quick-DNA Fungal/Bacterial Miniprep Kit (Zymo Research, USA, #D6005), plasmid isolation and PCR product extraction from agarose gels were carried out using GeneJET kits (Thermo Fisher Scientific, USA, #K0503, #K0832). Site-directed mutagenesis was carried out using Phusion™ Plus DNA Polymerase (Thermo Fisher Scientific, USA, #F631XL) and a single oligonucleotide primer as described in (60). Codons encoding amino acids of interest were changed to ones either encoding methionine or alanine (61). An empty pLATE11 vector was created by PCR amplification of the backbone and blunt end ligation.

Cultivation of bacteria and overexpression of recombinant proteins

For the bacterial growth assay, *E. coli* HMS174 Δ*pyrF* strains, either carrying the pLATE11 vector with an insert or an empty pLATE11 vector as a negative control, were initially cultured in LB medium supplemented with 100 μg/ml ampicillin overnight at 37 °C, 180 rpm. The overnight cultures were subsequently diluted in M9 minimal media (1× M9 salts, 1 mM $MgSO_4$, 0.05 mM $CaCl_2$, 0.4% glucose, 100 μg/ml ampicillin, 0.1 mM IPTG) uniformly to OD_{600} 0.001. If necessary, inoculates were supplemented with nucleobases at the final concentration of 200 μM, and 150 μl of suspensions were dispensed into the wells of 96-well flat-bottom plate. Bacterial growth was monitored using Infinite M200 PRO (Tecan, Switzerland) microplate reader. Plates were incubated at 37 °C with periodic shaking for 30 s every 5 min and OD_{600} measurements every 15 min.

For tRNA isolation, a single colony of *E. coli* BL21(DE3), either carrying the pLATE11 vector with an insert or an empty pLATE11 vector as a negative control, was inoculated into 20 ml of LB medium supplemented with 100 μg/ml ampicillin. Cultures were incubated at 37°C, 180 rpm. Upon reaching the log phase (OD_{600} ~0.6), the production of recombinant protein was induced by the addition of IPTG to a final concentration of 0.1 mM. Cells were harvested by centrifugation 4 h post-induction and used for tRNA isolation immediately or stored at −20°C until further use.

For protein purification, an auto-induction medium with slight modifications was used (62). The base of the medium consisted of 10 g tryptone, 10 g yeast extract and 10 g glycerol per 1 l of medium. The medium was supplemented with 50× salt solution (1.25 M Na_2HPO_4, 1.25 M KH_2PO_4, 2.5 M NH_4Cl, 0.25M Na_2SO_4), 50× lactose solution (25% glycerol, 2.5% glucose, 10% α-lactose), $MgSO_4$ (2 mM final concentration), 1000× trace metal solution, and 100 μg/ml ampicillin. A single colony of *E. coli* BL21(DE3) carrying pLATE52 vector with an insert was inoculated into 50 ml of medium and incubated at 37 °C, 180 rpm. After 6 h, the temperature was reduced to 20°C, and the incubation continued for an additional 16–20 h. To verify induction, 1 μl of a 2% X-Gal solution was added to 1 ml of the culture, followed by incubation for 30 min at 37 °C.

Phylogenetic analysis

The tRNA sulfurtransferase P77718 (63) from *E. coli* was selected as the representative sequence for ThiI, and A0A2L1IC02 (63) from *Pseudomonas* sp. SWI36 was selected as the representative sequence for RudS. These sequences were used to obtain homologous sequences for seed alignments using HMMER (64) with the n70 and nr90 databases (MPI Bioinformatics Toolkit (65)). The initial sequences were split according to domain boundaries identified from AlphaFold2

Table 1. TudS, RudS, and DUF1722 encoding genes used in this study

Insert	Domain structure	Origin	GeneBank accession ID (87)	Gene locus tag	Conserved cysteines
RudS_KT	TudS-DUF1722	*Pseudomonas putida* KT2440	AE015451	PP_0741	Cys17, Cys49, Cys114
RudS_TT	TudS-DUF1722	*Thermus thermophilus* HB8	AP008227	TTHB112	Cys16, Cys47, Cys111
RudS_ST[a] (ORF319)	TudS-DUF1722	*Salmonella enterica* subsp. *enterica* LT2	AE006468	STM1389	Cys12, Cys44, Cys110
RudS_PU	TudS-DUF1722	*Pseudomonas* sp. MIL9	JAFEHE010000014	JQF37_16640	Cys15, Cys47, Cys112
RudS_PP	TudS-DUF1722	*Pseudomonas* sp. MIL19	JAPPVG010000016	N1078_12140	Cys18, Cys50, Cys115
RudS_vir	TudS- DUF1722	*Escherichia* phage 1H12	NC_049947	H3V29_gp66	Cys12, Cys44, Cys110
TudS	TudS	Uncultured bacterium	6Z92_A (39,40,58)	–	Cys10, Cys43, Cys104
YbgA	DUF1722	*Escherichia coli* DH5α	NZ_SGJA00000000	b0707	–

[a]The RudS protein from *Salmonella enterica* (RudS_ST here) was previously referred to as ORF319 in the literature (88).
The conserved cysteine residues are predicted to form the iron-sulfur cluster within the active center of the TudS domain.

models, specifically the THUMP, ThiI and Rhodanese-like domains in ThiI, and the TudS and DUF1722 domains in RudS.

Sequences for each domain obtained from the HMMER search were realigned using T-CoffeeWS with default settings. These alignments were then used to construct hidden Markov models (HMMs). HMMSEARCH was employed to search for homologous sequences using the previously constructed HMMs among complete reference genomes of 332 Archaea, 5042 Bacteria and 47 viruses. The criteria for the presence of RudS in genomes were an e-value <0.001 and an aligned region length with the HMM >80 amino acids for both the TudS and DUF1722 domains, with these domains appearing in this specific order. The same criteria were applied for the ThiI search, but only the THUMP and ThiI domains were required, instead of all three domains present in P77718.

Found RudS homologues were aligned using HMMALIGN with HMMs produced from the seed alignments obtained with HMMER, as previously described for domain alignments. The resulting alignment was used to produce a phylogenetic tree using Biopython (66) capabilities, with identity fraction as the distance metric and the UPGMA method (67). The resulting tree was visualized using the ETE toolkit (68).

Preparation of bulk tRNA

Bulk tRNA was prepared with slight modifications to the method described in (69). Harvested *E. coli* BL21(DE3) bacterial culture was resuspended in 600 µl of extraction buffer (1 mM Tris–HCl, pH 7.4, 10 mM Mg-acetate) and mixed with 600 µl of ROTI Aqua-Phenol (Carl Roth, Germany, #A980.3). The mixture was mixed using a vortex mixer at 2000 rpm for 15 min, followed by centrifugation at 30 000 *g*, 16°C for 10 min. The aqueous phase was mixed with 0.1 volume of 5 M NaCl and 2 volumes of 100% ethanol, followed by centrifugation at 30 000 *g*, 4°C for 10 min. The pellet was resuspended in 550 µl of 1 M NaCl and centrifuged at 30 000 *g*, 4°C for 10 min. Subsequently, 500 µl of the supernatant was mixed with 1250 µl of 100% ethanol and incubated at –20°C overnight. The precipitate was collected by centrifugation at 30 000 *g*, 4°C for 10 min and dissolved in 25 mM K-phosphate buffer (pH 6.5).

For the purification step, the sample was applied to a HiTrap DEAE Sepharose FF column (Cytiva, USA, #17505501) pre-equilibrated with buffer A (25 mM Na-phosphate pH 6.5, 50 mM NaCl, 5 mM $MgSO_4$) using AKTA Pure FPLC system (Cytiva, USA). The tRNA was eluted by applying a linear gradient (0–100%) of buffer B (25 mM Na-phosphate pH 6.5, 1 M NaCl) over 10 min using 10 CV. The eluted fractions were precipitated by the addition of 3 volumes of 100% EtOH. The resulting pellet was resuspended in DEPC-treated water.

Nano-tRNAseq

The nano-tRNAseq of total *E. coli* BL21(DE3) tRNA was performed by Immagina Biotechnology S.r.l. (Italy) using a nanopore-based sequencing approach (70). The bulk tRNA was extracted as indicated above and s4U was quantified using HPLC-MS/MS.

tRNA digestion and analysis of modified nucleosides

For the analysis of modified nucleosides using HPCL-MS/MS, 1 µg of tRNA was heat denatured for 5 min at 95°C and subjected to digestion at 37°C for 16 h using Nucleoside Digestion Mix (New England BioLabs, USA, #M0649S). After digestion, proteins were precipitated by adding an equal volume of acetonitrile to the digested tRNA. The mixture was mixed at 1400 rpm, 37°C for 10 min, and centrifuged at 30 000 *g*, 4°C for 20 min. The supernatant was used for nucleoside analysis.

4 µl of the supernatant were analyzed using liquid chromatography-tandem mass spectrometry with a Nexera X2 UHPLC system coupled with LCMS-8050 mass spectrometer (Shimadzu, Japan) equipped with an ESI source. The chromatographic separation was carried out using a 3 × 150 mm YMC-Triart C18 (particle size 3 µm) column (YMC, Japan, #TA12S03-1503WT) at 40°C and a mobile phase that consisted of 0.1% formic acid (solvent A) and acetonitrile (solvent B) delivered in gradient elution mode at a flow rate of 0.45 ml/min. The following elution program was used: 0 to 1 min, 5% solvent B; 1 to 5 min, 95% solvent B; 5 to 7 min, 95% solvent B; 7 to 8 min, 5% solvent B; 8 to 12 min, 5% solvent B. Modified nucleosides were detected using transitions *m/z* 247→115 (dihydrouridine), 261→129 (4-thiouridine) and 260→94 (2-thiocytidine) at interface temperature of 300°C and desolvation line temperature of 250°. N_2 was used as nebulizing (3 l/min) and drying (10 l/min) gas, dry air was used as heating (10 l/min) gas. The data were analyzed using LabSolutions LCMS software. For quantification, the amount of 4-thiouridine was normalized to the total dihydrouridine content (71).

Western blot analysis

In total, 2 ml of induced bacterial cultures (see "Cultivation of bacteria and overexpression of recombinant proteins") were centrifuged, and the pellets were resuspended in 2 ml Tris–HCl pH 7, 250 mM NaCl buffer. Cells were disrupted using an ultrasonic disintegrator and centrifuged at 30 000 *g*, 4°C for 10 min. The concentrations of the soluble fractions of the crude extracts were measured using Pierce Bradford Assay Kit (Thermo Fisher Scientific, USA, #23246). All samples were adjusted to a concentration of 200 ng/μl, and 2 μg of soluble crude extract was loaded onto a 14% SDS-PAGE gel using the Bio-Rad Mini-PROTEAN electrophoresis system and a 10-well or 15-well, 0.75 mm comb (Bio-Rad, USA, #1653355). Following the electrophoresis, proteins were transferred onto a 0.45 μm nitrocellulose membrane (Thermo Scientific, USA, #88018) and blocked using TBST (10 mM Tris–HCl pH 7.5, 150 mM NaCl, 0.1% Tween 20) containing 0.2% I-Block reagent (Thermo Fisher Scientific, USA, #T2015) for 1 h at room temperature. The membrane was incubated overnight at 4°C with anti-His-Tag antibodies (Thermo Fisher Scientific, USA, #MA1-21315) diluted 1:1000 in the blocking solution. The following day, membranes were incubated with the HRP-conjugated anti-mouse secondary antibody (Carl Roth, Germany, #4759) diluted 1:10 000 in blocking solution for 1 h at room temperature. Detection of protein-antibody complexes was performed using an enhanced chemiluminescence substrate (Thermo Fisher Scientific, USA, #32209) and digitally imaged with Azure 280 chemiluminescence detection system (Azure Biosystems, USA). Band intensities were quantified using ImageJ software (National Institutes of Health, USA).

Purification of RudS_KT recombinant protein

Cells from 50 ml of induced *E. coli* BL21(DE3) cultures (see "Cultivation of bacteria and overexpression of recombinant proteins") were resuspended in 7.5 ml of buffer A (50 mM Tris–HCl pH 8, 500 mM NaCl, 10 mM imidazole, 10% (w/v) glycerol), supplemented with ∼0.1 mg of DNase I (Roche, Switzerland, #10104159001), 15 mM $MgSO_4$ and 1mM PMSF. Cells were disrupted using an ultrasonic disintegrator and centrifuged at 30 000 *g*, 4°C for 10 min. The supernatant was applied to 1 ml HiTrap Chelating HP chromatography column (Cytiva, USA, #17040801) pre-equilibrated with buffer A using AKTA Pure FPLC system (Cytiva, USA).

The protein was eluted by applying a linear gradient (0–100%) of buffer B (50 mM Tris–HCl pH 8, 500 mM NaCl, 500 mM imidazole, 10% (w/v) glycerol) over 10 min using 10 CV. Following elution, the buffer in the fractions was exchanged with buffer S (50 mM Tris–HCl pH 8, 500 mM NaCl, 10% (w/v) glycerol) using 5 ml HiTrap Sephadex G-25 Desalting columns (Cityva, USA, # 17140801).

To minimize the protein's exposure to oxygen, all buffers were degassed under vacuum for 30 min with stirring. The fractions were collected in 0.5 ml aliquots in 0.5 ml tubes and sealed immediately after fractionation.

Purified protein samples were analyzed using 14% SDS-PAGE gel, protein concentration was measured using Pierce™ Bradford Protein Assay Kit (Thermo Fisher Scientific, USA, #23200), protein spectrum analysis was carried out using GENESYS™ 150 UV–Vis Spectrophotometer (Thermo Fisher Scientific, USA), iron content in protein samples was determined using ferene (Merck, Germany, #P4272) and $FeCl_2$ as a standard (72).

Determination of RudS_KT molar mass

The molar mass of RudS_KT was determined by analytical gel filtration using a Superose 12 10/300 GL column (Cytiva) previously equilibrated with 50 mM Tris–HCl pH 8, 500 mM NaCl, 10% (w/v) glycerol, under aerobic conditions. Carbonic anhydrase (29 kDa), bovine serum albumin (66 kDa), alcohol dehydrogenase (150 kDa), and β-Amylase (200 kDa) were used as standards (Sigma-Aldrich, USA, #1002033699) for column calibration. The experiment was repeated three times to determine the standard deviation.

In vitro activity assay

In vitro tRNA 4-thiouridine desulfidation assay was carried out aerobically using purified RudS_KT and total tRNA from *E. coli* MRE 600 (Roche, Switzerland, #10109541001). Purified RudS_KT concentrations were adjusted to 0.7 mg/ml (17.85 μM) with buffer S (50 mM Tris–HCl pH 8, 500 mM NaCl, 10% (w/v) glycerol). Reactions were carried out in 100 μl reaction mixtures containing 5.3 μM RudS_KT, 0.4 μM tRNA, 100 mM Tris–HCl pH 7 and 150 mM NaCl at 22°C. Reactions were stopped by heating the samples at 95°C for 5 min followed by centrifugation at 30 000 *g*, 4°C for 10 min, and ethanol precipitation of tRNA in supernatant. Samples were digested to single nucleosides and analyzed by HPLC-MS/MS as described above.

To test the (p)ppGpp effect on RudS_KT activity, 10 fold molar excess of guanosine-3′,5′-pentaphosphate (pppGpp) (Jena Bioscience, Germany, #NU-885S) or guanosine-3′,5′-tetraphosphate (ppGpp) (Jena Bioscience, Germany, #NU-884S) was added to equimolar amount of tRNA and RudS_KT. Reactions were carried out in 100 μl reaction mixtures at 22°C containing 4 μM RudS_KT, 4 μM tRNA, 100 mM Tris–HCl, pH 7, 150 mM NaCl and 40 μM of (p)ppGpp. Reactions were stopped by heating and analyzed as described above.

Electrophoretic mobility shift assay (EMSA)

Non-radioactive EMSA was adapted from (73) with slight modifications. The binding reaction was carried out in 20 μl volume and contained 20 mM Tris–HCl, 10% glycerol, 200 mM NaCl, 0.5 μg (1 μM final concentration) total *E. coli* tRNA and 6 μM his-tagged *E. coli* pseudouridine synthase TruB (positive shift-control) or 1–10 μM RudS_KT. After 1 min incubation on ice, the whole binding mixture was loaded into 2% agarose gel prepared by using RNase-free TBE buffer (Invitrogen, USA) and DEPC-treated water. Gel and TBE running buffer was supplemented with SYBR™ Green II RNA Gel Stain (Invitrogen, USA, S7564). The gel was run at 7 V/cm for 90 min and imaged using Azure 280 fluorescence detection system (Azure Biosystems, USA).

Modelling and molecular dynamic simulations

The RudS_KT structures were modeled using Alphafold2 (74) and trRosetta (75) web servers. Both methods utilized multiple sequence alignments generated with mmseqs2 (76) and HHblits (77) for Alphafold2 and trRosetta, respectively. The RudS_KT holoenzyme model was constructed by selecting the best model from Alphafold2 and incorporating the iron-sulfur cluster from PDBID: 6z96 (58). Molecular dynamics calculations were performed using the AMBER20 software package (78). The holoenzyme model was parameterized with the

AMBER ff14SB force field (79) and the TIP3P explicit solvent model with a 12 Å protein water solvation box and approximately 150 mM NaCl. The angle and bond parameters for the iron-sulfur cluster were adapted from (80), with charges adjusted for different iron oxidation states.

A crystal structure of *E. coli* phenylalanine tRNA (PDBID:6y3g) (81) served as the model substrate, featuring a 4-thiouridine moiety at the 8th position. As the original structure rendered the thiouridine moiety inaccessible to the enzyme, we manually repositioned the base to obtain an initial substrate structure suitable for enzymatic interaction. Additionally, calcium ions in the crystal structure were replaced with magnesium ions. Both the original and repositioned structures were parameterized using identical water models and ranges as the protein, supplemented with OL3 and modrna8 force field for modified RNA (82–84).

The initial enzyme-substrate structures were docked using default settings on the HDOCK web server (85). The resulting structures were ranked based on the distance between the sulfur atom in the thiouridine moiety and the relevant iron atom in the iron-sulfur cluster. The structure that performed best in this regard was selected for further calculations. Molecular dynamics simulations, with various restraints detailed in the Supporting Information, were carried out for the holoenzyme, tRNA substrates, and enzyme-substrate complexes.

Ultraviolet A (UVA) irradiation experiments

A single colony of *E. coli* BL21(DE3), either carrying the pLATE11 vector with an insert or an empty pLATE11 vector as a negative control, was inoculated into 20 ml of LB medium supplemented with 100 μg/ml ampicillin and incubated at 37 °C, 180 rpm overnight. The next day 200 μl of overnight culture was inoculated into 20 ml of fresh of LB medium supplemented with 100 μg/ml ampicillin and incubated at 37 °C, 180 rpm. Upon reaching the log phase (OD_{600} ~0.6), the production of recombinant protein was induced by the addition of IPTG to a final concentration of 0.1 mM. Two hours post-induction, the cells were transferred on ice followed by OD_{600} measurements. The cultures were subsequently diluted in cold M9 minimal media (1× M9 salts, 1 mM $MgSO_4$, 0.05 mM $CaCl_2$, 0.4% glucose, 100 μg/ml ampicillin, 0.1 mM IPTG) uniformly to OD_{600} 0.05 and 150 μl of suspensions were dispensed into the wells of pre-cooled 96-well flat-bottom plate. The UVA irradiation was carried out in UVP C-10 Chromato-Vue cabinet (Analytik Jena, Germany) equipped with 6W, 365 nm UVP UVGL-58 lamp (Analytik Jena, Germany). Bacterial suspensions were irradiated for 120 min (theoretical exposure ~100 kJ/m^2), the plate was held on ice throughout the whole procedure. Subsequently, bacterial growth was monitored using Infinite M200 PRO (Tecan, Switzerland) microplate reader. Plates were incubated at 37 °C with periodic shaking for 30 s every 5 min and OD_{600} measurements every 15 min.

Results

TudS and RudS proteins do not share the same phenotype in vivo

Our recent research revealed that a family of widespread bacterial proteins consisting of a stand-alone TudS domain (formerly DUF523) salvage thiolated uracil derivatives with the highest preference for thiouridine monophosphate (4-thio-UMP), which most likely emanates from cellular tRNA degradation (40). Although the single-domain TudS proteins are predominant in this family of proteins (9436, or 58.9% of all reported sequences), a significant portion is found fused with the DUF1722 domain (6425, or 40.1% of all reported sequences) (86). Notably, the *P. putida* KT2440 genome encodes for both a stand-alone TudS (GenBank gene locus ID: PP_5158) and a TudS-DUF1722 fusion protein RudS (GenBank gene locus ID: PP_0741). Gene knockout studies in *P. putida* KT2440 suggested that contrary to stand-alone TudS (PP_5158) the RudS (PP_0741) gene product does not participate in exogenous 4-thiouracil/4-thiouridine utilization (40), which prompted the question whether a TudS-DUF1722 fusion protein could have an alternative substrate to that of a stand-alone TudS.

To confirm that RudS fusion proteins' activity in vivo is different from stand-alone TudS, we firstly cloned and overexpressed the *P. putida* PP_0741 gene (RudS_KT) product in uracil auxotrophic *E. coli* HMS174 Δ*pyrF*, replicating conditions of our previous studies (39,40,58). Using liquid M9 media we observed the growth restoration on 4-thiouracil (Figure 1D), albeit after an extended lag phase compared to TudS (Figure 1B). No growth was observed on 2-thiouracil, unlike with previously characterized TudS proteins. These findings suggested that RudS_KT exhibits residual activity towards thiolated uracil compounds as substrates.

We cloned four additional RudS genes from common laboratory strains and soil bacteria (Table 1). Notably, *Escherichia coli* lacks the TudS or RudS homologues, but possesses a stand-alone DUF1722 domain encoding gene *ybgA*, which was tested as well (Figure 1C). Ten gene sequences of viral origin RudS were reported, all within the *Siphoviridae* family (86), of which we chose the RudS_vir from *Escherichia* phage 1H12 for further analysis (Figure 1I).

The stand-alone TudS gene product (Figure 1B) served as a positive control for this experiment, while the stand-alone DUF1722 gene product (Figure 1C) exhibited similar behavior to the negative control (Figure 1A). None of the tested RudS variants supported the growth of the uracil-auxotroph in the same manner as TudS. Similarly to RudS_KT (Figure 1D), bacteria with RudS from other *Pseudomonas* species (Figure 1F,H) displayed a significant lag phase before initiating growth on 4-thiouracil, while viral-origin RudS showed the shortest lag phase on 4-thiouracil (Figure 1I). In contrast, the RudS_TT from *Thermus thermophilus* (Figure 1G) and RudS_ST from *Salmonella enterica* (Figure 1E) were unable to rescue the uracil auxotrophic strain on either 4- or 2-thiouracil. None of the tested RudSes supported the growth on 2-thiouracil. The growth curves suggested that thiolated uracils are not the primary substrates for RudS variants, as they did not exhibit significant activity towards these compounds.

Phylogenetic analysis indicates a link between ThiI and RudS

Observation of either promiscuous or absent TudS-like activity in RudS suggested that TudS and RudS likely have distinct functions in vivo. However, the presence of the TudS domain within RudS implies a potential role related to 4-thiouridine desulfidation. This assumption is supported by the fact that genes encoding the DUF1722 domains are conserved in prokaryotes, as well as are the genes encoding ThiI, the

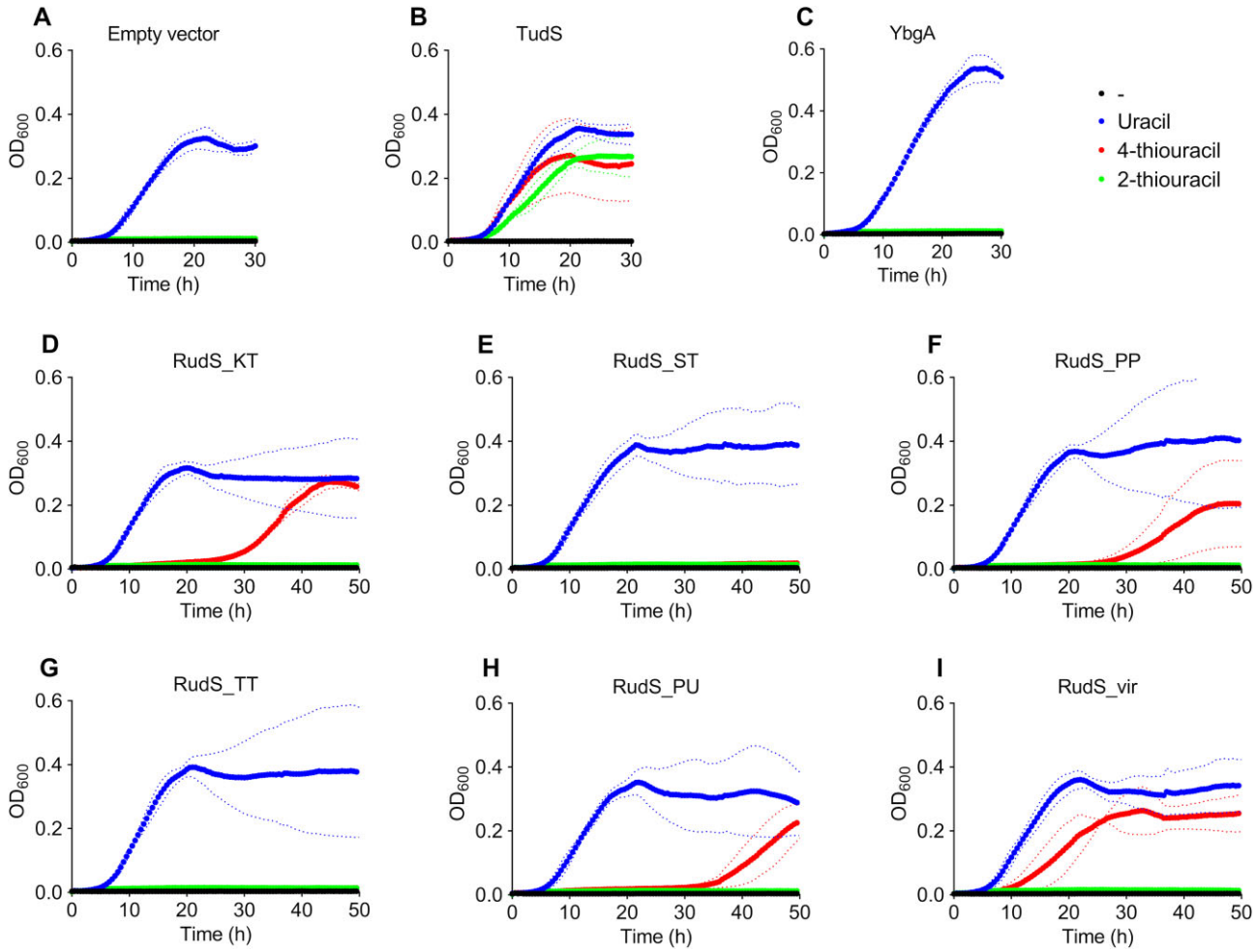

Figure 1. Growth curves of uracil auxotrophic *E. coli* HMS174 Δ*pyrF* expressing TudS, RudS, and DUF1722 domain encoding genes in the presence of uracil (blue), 2-thiouracil (green) and 4-thiouracil (red). Dotted lines represent standard deviation. (**A**) Empty vector carrying bacteria (negative control). (**B**) TudS producing bacteria (positive control). (**C**) YbgA (stand-alone DUF1722 domain) producing bacteria. (**D**) RudS_KT producing bacteria. (**E**) RudS_ST producing bacteria. (**F**) RudS_PP producing bacteria. (**G**) RudS_TT producing bacteria. (**H**) RudS_PU producing bacteria. (**I**) RudS_vir producing bacteria.

enzyme responsible for s4U synthesis. PhyloCorrelate analysis (89) of bacterial and archaeal genes revealed a notable pattern: most species with the DUF1722 domain gene also encode the ThiI gene (94% of DUF1722 encoding species). To further investigate this potential connection, we performed a phylogenetic analysis and obtained the results shown in Figure 2.

RudS homologous proteins (857) were identified among 884 reference genomes (843 Bacteria and 41 Archaea). ThiI homologous proteins were found among 1866 genomes. In 637 genomes, both full RudS and ThiI proteins are present (Figure 2, Supplementary Figure S1 for convenience). Although there are sporadic instances where ThiI is not present in the same genome, there are also two distinct groups of organisms that lack the ThiI homologue used in this analysis (Figure 2, Groups A and B). Group B mostly consists of thermophilic sulfate-reducing bacteria. Group A is very diverse, encompassing different morphologies and metabolic processes. We hypothesize that the organisms in these groups might possess ThiI homologues that differ in architecture from the *E. coli* homologue used to create this tree. Additionally, it is possible that they may not have the s4U modification altogether, but still retain the RudS enzyme. In conclusion, the phylogenetic analysis of RudS homologues from bacteria and archaea with known complete genomes confirmed that most organisms with a RudS gene also encode ThiI, reinforcing the link between these two enzymes.

Heterologous overexpression of RudS genes results in decreased 4-thiouridine content of *E. coli* tRNA

Given that 4-thiouridine, to the best of our knowledge, is conserved in tRNA, we decided to overexpress the RudS homologs in *E. coli*, isolate bulk tRNA, and examine its 4-thiouridine content.

Genes listed in Table 1 were overexpressed in *E. coli* BL21(DE3) cells, total tRNA was extracted from these cells, and the level of s4U in it was quantified using HPLC-MS/MS. A substantial decrease in s4U content, ranging from 4.7- to 26-fold, was observed in tRNA samples from cells overexpressing RudS encoding genes (Figure 3A). Conversely, overexpression of stand-alone TudS or YbgA (stand-alone DUF1722 domain) encoding genes did not exhibit any statistically significant effect on the s4U content of total tRNA compared to control samples (Figure 3A). Additionally, we investigated RudS's effect on other sulfur-modified nucleosides found in tRNA. We were unable to detect 2-thiouridine in our samples, likely be-

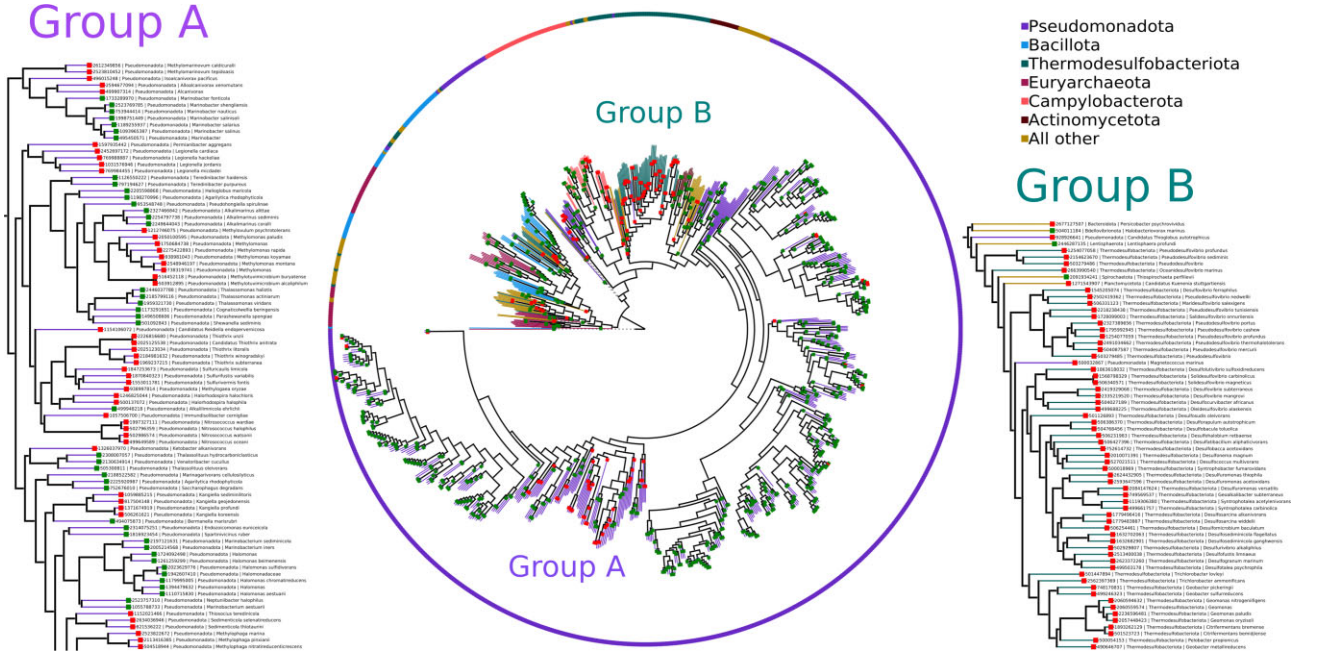

Figure 2. Phylogenetic tree of 884 RudS homologues identified among complete reference genomes of 332 Archaea, 5042 Bacteria, and 47 viruses. The presence (green square) or absence of ThiI (red square) in the same genome is indicated. Group A and Group B mark organism groups that lack the *E. coli* ThiI homologue.

cause this modification is conserved in only a few species of *E. coli* tRNA and is found in the Wobble position, where it is often hypermodified (90). However, we detected 2-thiocytidine, which is commonly located at position 32, adjacent to the anticodon (91), but observed no significant changes in its levels upon RudS induction (Supplementary Figure S2).

Among the six overexpressed RudS orthologs, the most significant decrease in s4U content (26-fold, compared to the negative control) was observed with RudS_KT from *Pseudomonas putida* KT2440, followed by RudS_ST from *Salmonella enterica* (18.3-fold), while RudS_PU from *Pseudomonas* sp. MIL9, overexpression resulted in the smallest decrease (4.7-fold). The variation in s4U content reduction among different RudS proteins raises the question of whether this was due to differences in heterologous expression levels or the specificity of RudS. To evaluate the levels of soluble proteins produced in *E. coli*, His-tags were introduced to the N-termini of RudS proteins for detection with anti-His-Tag antibodies.

Western blot analysis revealed that RudS_KT, while causing the most significant reduction in tRNA s4U content (Figure 3A), did not demonstrate the highest protein levels in the cells (Supplementary Figure S3A). In contrast, RudS_TT showed over 1.7-fold higher expression levels, but a lower s4U content reduction (8.7-fold, Figure 3A). The lower desulfidation activity of RudS_TT might be attributed to suboptimal temperature conditions for a protein originating from a thermophilic organism. It might also be due to inefficient substrate recognition, as tRNAs in thermophilic microorganisms often possess unique body modifications not found in their mesophilic counterparts (92). The detected soluble fractions of RudS_ST and RudS_PP were lower in comparison to RudS_KT (Supplementary Figure S3A), aligning with the observed reduction of s4U content (Figure 3A). Despite the undetectable level of soluble protein, a reduction in tRNA s4U content was observed with RudS_PU overexpression (Figure 3A). RudS_vir, on the other hand, stood out with relatively high protein levels (Supplementary Figure S3A), comparable to those of RudS_ST, yet its tRNA desulfidation activity appeared to be lower (Figure 3A). All tested RudS variants exhibited activity towards tRNA, indicating that RudS enzymes function as tRNA de-modifying erasers, targeting the 4-thiouridine modification in tRNA molecules.

The growth restoration of uracil auxotrophic cells (Figure 1) and characteristics of the TudS domain (40,58) suggest that RudS converts the s4U modification to uridine *in vivo*. To confirm this, we sequenced total tRNA extracted from control and RudS_KT overexpressing cells using nanopore-based nano-tRNAseq (70). Although this method could not distinguish the modified s4U residue in control samples, the sequencing results of RudS_KT-affected samples indicated the presence of uridine at the 8(9)th position. Combining these data with previous findings, we propose that RudS catalyzes the conversion of tRNA s4U to uridine.

An active [4Fe–4S] cluster is needed for *in vivo* tRNA desulfidation by RudS

Previously we uncovered the mechanism of 4-thiouracil-containing compound desulfidation by TudS (40,58). The key component in this process is a [4Fe–4S] cluster harbored in the enzyme's active center, bound by three cysteine residues, with the fourth iron atom engaging in substrate binding. Given that the overexpression of YbgA (the *E. coli* stand-alone DUF1722 domain) had no impact on tRNA s4U content (Figure 3A), we hypothesized that the TudS domain in the RudS fusion proteins should be responsible for the observed decrease of s4U in tRNA samples. We identified conserved cysteine residues (Figure 3B) which are likely to be involved in [4Fe–4S] cluster formation (Table 1), created single amino acid substitu-

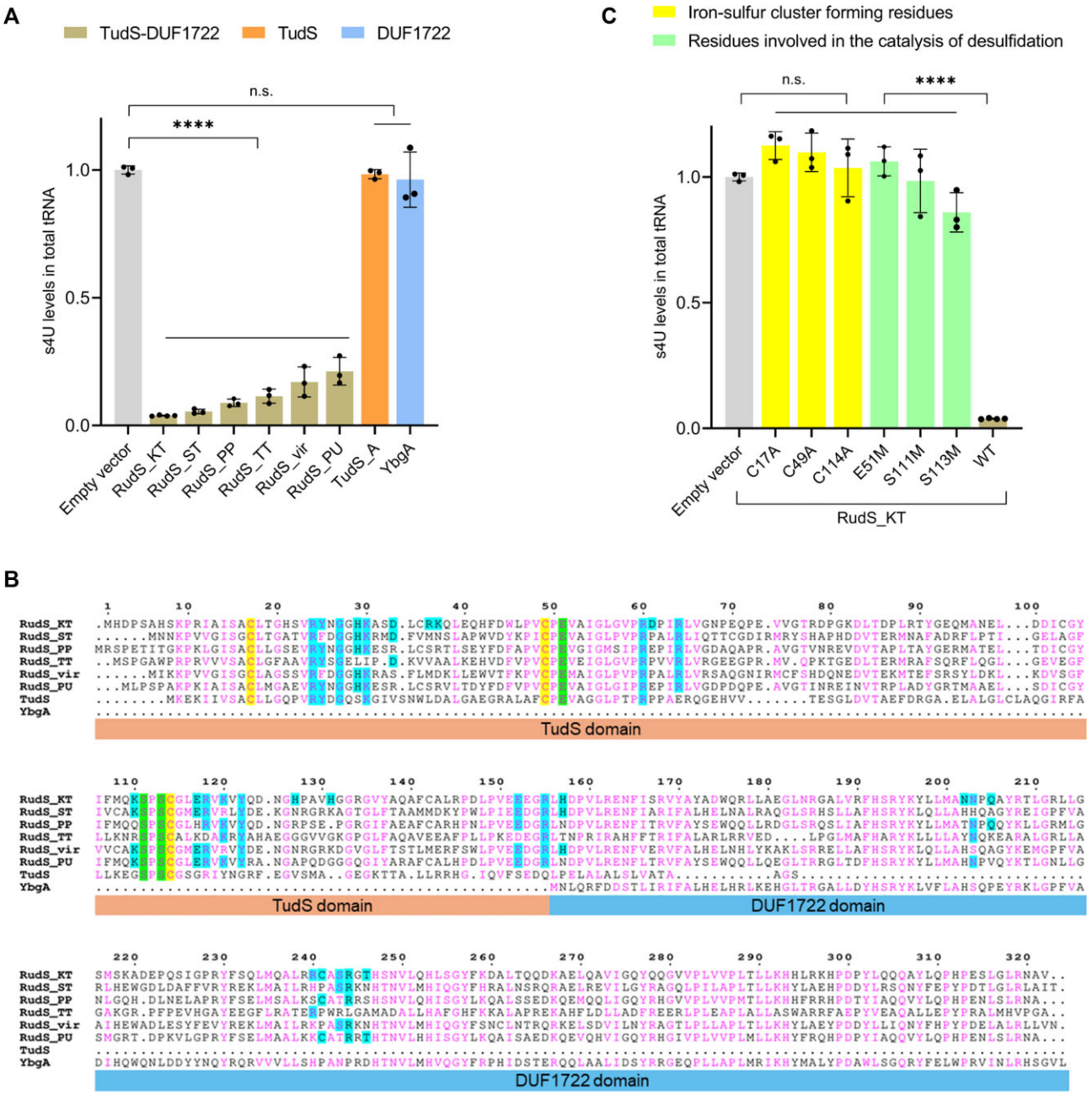

Figure 3. RudS reduces the s4U content of tRNA in vivo. (**A**) s4U levels in *E. coli* total tRNA upon expression of RudS, TudS and DUF1722 encoding genes. **** $P < 0.0001$, n.s.: $P \geq 0.05$ compared to negative control (empty vector), one-way ANOVA with Dunnet's post hoc test. (**B**) Sequence alignment of investigated RudS orthologs, TudS, and YbgA (stand-alone DUF1722 domain). Conserved cysteine residues involved in iron–sulfur cluster formation are highlighted in yellow. Conserved glutamic acid and serine residues catalyzing the 4-thiouridine desulfidation reaction are highlighted in green. Amino acids predicted in tRNA binding and/or catalysis are highlighted in cyan. (**C**) s4U levels in *E. coli* total tRNA upon expression of RudS_KT with single amino acid substitutions in conserved iron–sulfur cluster forming and catalytical residues. **** $P < 0.0001$, n.s.: $P \geq 0.05$ compared to negative control (empty vector) or wild-type RudS_KT (WT), one-way ANOVA with Dunnet's post hoc test.

tions of these cysteines in RudS homologues, and tested their tRNA desulfidation activity. Western blot analyses of His-tagged variants of mutant RudS proteins in the soluble fractions of the bacterial lysates indicated that the amounts of the mutant RudS protein variants are up to ∼4-fold lower than those of the wild types (Supplementary Figure S3B). The majority of mutant RudS protein variants showed a loss of activity (Figure 3C and Supplementary Figure S4), failing to significantly reduce s4U levels in *E. coli* tRNA, thus confirming our hypothesis. A single exception was the RudS_TT C47A protein variant (Supplementary Figure S4), which reduced the tRNA s4U content to levels comparable with those of the wild type RudS_TT. This suggests that a protein lacking one of the three cysteines might still form an active Fe–S cluster using only two cysteine ligands, a phenomenon previously reported in *Bacteroides thetaiotaomicron* fumarase. Despite lacking a typical third [4Fe–4S] cluster-coordinating cysteine found in bacterial fumarases, this enzyme remains active but is more prone to oxidative stress (93).

In vitro activity of RudS enzyme

Our previous studies showed that the iron-sulfur cluster in TudS is highly labile when exposed to oxygen, leading to an inactive enzyme when purified aerobically (39). Nevertheless, we produced N-terminally His-tagged RudS_KT in *E. coli* and purified it (Supplementary Figure S5A) under aerobic conditions with minimal oxygen exposure, as detailed in the methods section. On a molecular size exclusion chromatography column, RudS_KT eluted as a 37.1 ± 0.7 kDa protein (theoretical molar mass of ≈39 kDa), indicating a monomeric architecture (Supplementary Figure S5B). The recombinant protein exhibited a brown color typical for Fe–S cluster-containing proteins. Iron content determination using ferene assay indicated the presence of 1.01 ± 0.13 Fe per protein monomer, suggesting the major population of protein having damaged Fe–S cluster assumably caused by the exposure to oxygen. Despite the poor iron content, UV spectrum of purified protein demonstrated spectrum characteristic for [4Fe–4S] clusters, which was partially bleached upon treatment with dithionite (Supplementary Figure S5C).

Despite indications of a damaged [4Fe–4S] cluster, purified RudS_KT remained soluble over extended periods of time. To test direct tRNA binding, as is typical for tRNA modifying enzymes, we conducted an electromobility shift assay (EMSA) with *E. coli* pseudouridine synthase (TruB) serving as a positive shift control (94). EMSA revealed a concentration-dependent protein band shift, confirming the RudS_KT–tRNA complex (Figure 4A).

To ensure that RudS_KT is directly responsible for the observed decrease in tRNA s4U content, we performed an *in vitro* tRNA desulfidation reaction using total *E. coli* tRNA. Contrary to previous observations with TudS, the aerobically purified and desalted RudS_KT protein retained activity. An approximately 13-fold molar excess of aerobically purified RudS_KT reduced the 4-thiouridine content in tRNA by ∼80% over 1 min and by ∼95% over 1 h (Figure 4B). The desulfidation of the substrate was incomplete, likely due to the degradation of the remaining iron-sulfur clusters, although the inaccessibility of s4U due to non-physiological conditions or incorrect tRNA folding cannot be ruled out.

Additionally, we tested whether alarmones guanosine pentaphosphate and tetraphosphate influence RudS in vitro. We observed no statistically significant changes in the RudS enzymatic activity when using a 1:10 concentration ratio of RudS to (p)ppGpp (Supplementary Figure S6).

Docking studies reveal RudS amino acid residues involved in tRNA-binding

Due to challenges in crystallizing the RudS_KT, we employed molecular docking and MD simulations as an alternative approach to explore this proteins ability to desulfurize tRNAs. The MD simulations were conducted as described in the Materials and Methods and in the SI.

Figure 5A shows the superposition of the top five models generated by Alphafold2 and trRosetta (74,75), indicating substantial similarity among them. Figure 5B illustrates high modeling confidence levels (plDDT > 90) reported by both methods. Figure 5C presents a structural comparison with the closest identified homologue (HHpred (95); PDBID:6z96), revealing similarity in the organization of the TudS domain. The active center with the iron-sulfur cluster has identical amino acids, except Lys98 in TudS is replaced by Met108 in RudS_KT, suggesting a similar catalytic mechanism for desulfuration (58).

The RudS_KT holoenzyme model was built using the best Alphafold2 model and transferring the iron-sulfur cluster from PDBID:6z96 (58). The DUF1722 domain of RudS_KT consists of two compact groups of four alpha helices. No significant structural matches were found for this segment using the Dali structural homology search (96).

Two independent 160 ns MD simulations of the holoenzyme were conducted using randomly selected frames from the restraint relaxation MD simulation's trajectory. During the simulations, the DUF1722 domain was mobile relative to the catalytic domain. Therefore, for RMSD and principal component analysis, we focused on the compact part of the Ruds_KT catalytic domain (amino acids 11–168).

Figure 6A shows RMSD changes with the first structure as a reference. Both simulations exhibited a similar ∼1.7 Å RMSD drift, indicating convergence of the catalytic domain structure. PCA analysis (Figure 6B and C) and visual inspection of the superposition (Figure 6D) support this conclusion. The latter also includes the closest known structure of a homologous protein (TudS, PDBID: 6z96). The catalytic domain structure remained consistent throughout the simulations.

Key differences from TudS include an extended loop (amino acids 116–135) and a mobile loop (amino acids 18–33), also evident in the Alphafold2 and Rosetta models (Figure 5). We hypothesize that the mobility of these loops makes the enzyme's active center more open, allowing it to accommodate large substrates like tRNAs, at the expense of smaller substrates like thiouracil.

We also conducted a series of molecular dynamics simulations on a selected tRNA structure. A phenylalanine tRNA from *E. coli* with a thiouridine modification at the 8th position was chosen as the model substrate (PDBID: 6y3g) (81). The thiouridine moiety was initially buried and inaccessible for enzymatic attack. Since it was unlikely to flip out spontaneously during the MD simulation, we manually flipped this residue out and performed 500 ns MD simulations without any restraints, using the same methodology as for the holoenzyme.

The RMSD, PCA and structural comparison showed that the ribose and phosphate backbone remained stable throughout the simulation (Supplementary Figure S7). The last frames of these simulations were used to model the RudS–tRNA complexes.

Mutation analysis gives insight into the RudS–tRNA binding mechanism

The structures from previous MD simulations of the RudS holoenzyme and the tRNA with the exposed thiouridine were used for docking studies with HDOCK. Complexes were ranked based on the distance between the iron in the iron-sulfur cluster and the sulfur atom in the tRNA's thiouridine. The top 15 complexes are shown in Supplementary Figure S8, but none had iron-sulfur distances relevant for catalysis. However, these structures provided a preliminary hypothesis on how tRNA might bind to the holoenzyme. From these structures, we identified seven groups of amino acids (six groups G1–G6 for amino acids in each loop interacting with tRNA and a separate group CAT for catalytic amino acids) near the tRNA that might play a role in catalysis or substrate binding (Supplementary Table S4).

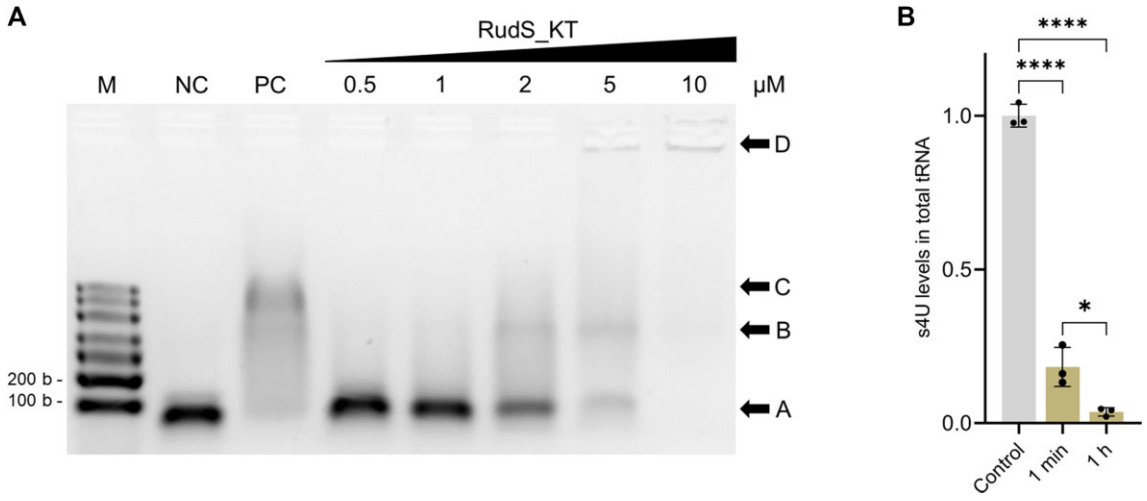

Figure 4. Purified recombinant RudS_KT interacts with tRNA *in vitro*. (**A**) Electrophoretic mobility shift assay. M – molecular marker, NC – tRNA control, PC – positive shift control (1:6 molar ratio, using *E. coli* TruB pseudouridine synthase); 0.5–10 μM or RudS_KT was added to binding mixture resulting in 1:1–1:20 tRNA–RudS_KT molar ratios. Arrowhead A indicates unbound tRNA, B – tRNA-RudS_KT complex, C – tRNA-TruB complex, D – gel wells. (**B**) Recombinant RudS_KT desulfidation activity in vitro using *E. coli* total tRNA. $****P < 0.0001$, $*P < 0.05$, one-way ANOVA with Bonferroni's post hoc test.

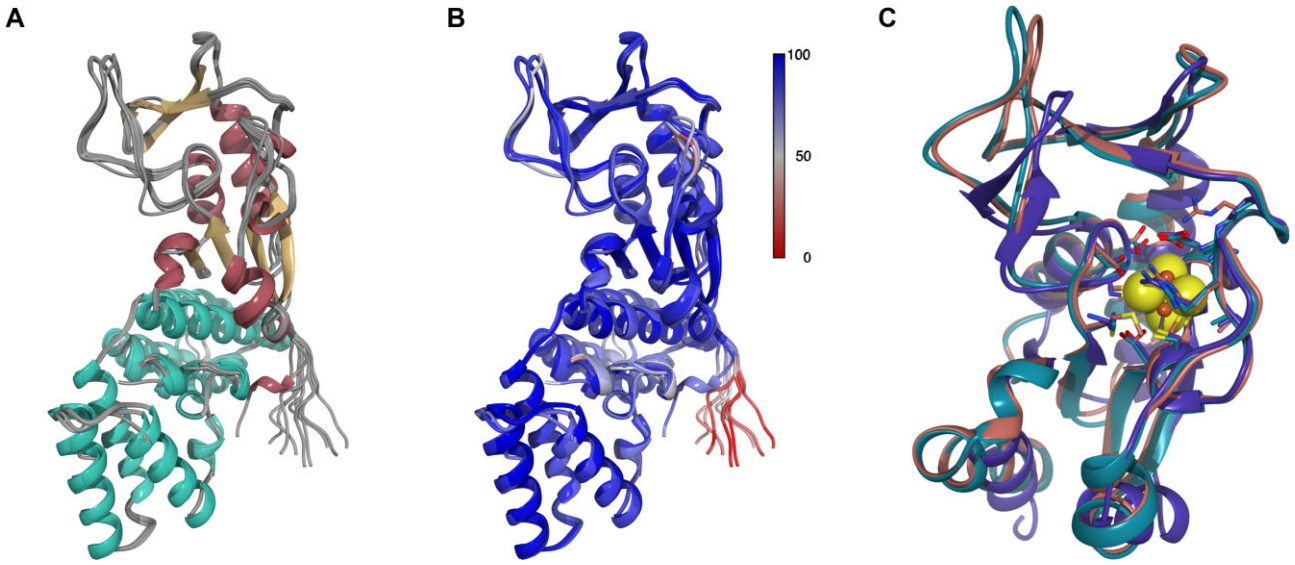

Figure 5. Structural comparison of RudS_KT models. (**A**) a superposition of Alphafold2 and RosettaFold models colored by secondary structure (alpha helices of DUF1722 domain are cyan). (**B**) models colored by pLDDT. (**C**) structural comparison of best Alphafold2 (teal) and trRosetta (salmon) models with closest homologue (PDBID:6z96) with structure identified with HHpred (purple). Iron-sulfur cluster is represented with spheres.

The best HDOCK structure was subjected to constrained MD simulations to position the thiouridine sulfur atom 2 Å away from the iron ion in the iron-sulfur cluster (S/Fe restraint). This complex was then used as the starting structure for two independent MD simulations. In the first simulation, the S/Fe restraint and additional restraints on catalytic distances were applied (model 1), while in the second only S/Fe restraint was maintained (details in Supporting Information). These simulations aimed to model the RudS-tRNA structure with a catalytically relevant substrate binding mode and to allow the complex to relax, better representing potential induced fit changes in the protein and tRNA structures.

We experimentally investigated these hypothesized catalytic amino acids by mutating them into methionines (Table 2). Mutations of proposed catalytic amino acids essentially abolished desulfidase activities (Figure 3C, Supplementary Figure S4), while other mutations had varying effects (Supplementary Figure S9). Each group contained at least one amino acid affecting enzymatic activity. These experimental results were compared to MD simulations of two holoenzyme-tRNA complex models (model 1 and model 2) described in the Supporting Information.

Figure 7A illustrates the superposition of the catalytic domains (amino acids 11–168) from the models and the holoenzyme, showing high similarity except for the previously discussed mobile loops, which are less mobile in the enzyme–substrate complex. Both models suggest that the DUF1722 domain interacts with the anticodon arm and anticodon of the tRNA, while the catalytic domain interacts with the variable loop, acceptor stem, and D arm of the tRNA. The DUF1722

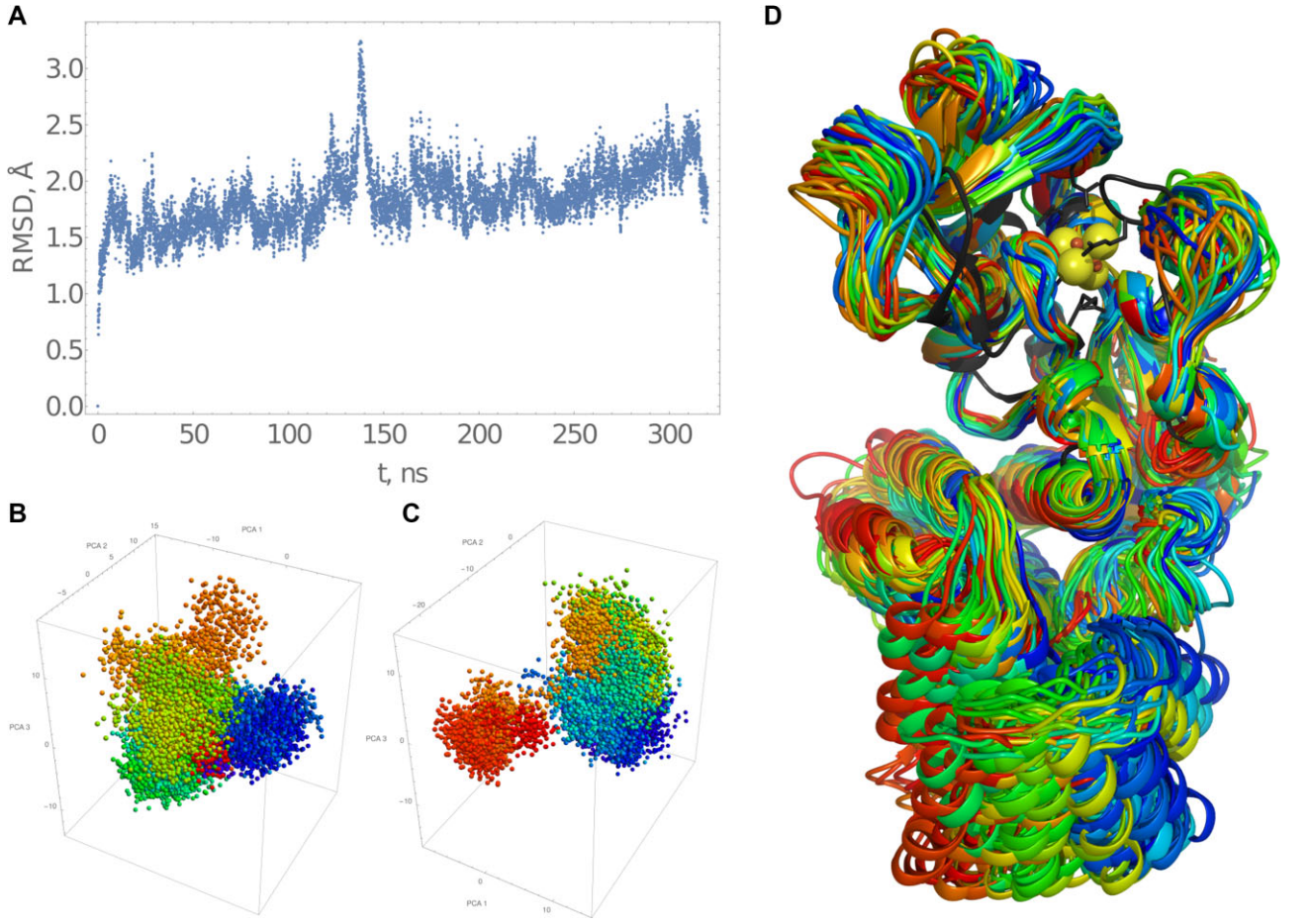

Figure 6. Molecular dynamics simulation of RudS_KT holoenzyme. (**A**) cumulative RMSD plot of two 160 ns MD simulations with different starting conformations. (**B** and **C**) PCA of both simulations. (**D**) superposition of complexes colored according to the PCA, the TudS protein (PDBID:6z96) is in black.

domain's mobility relative to the catalytic domain is evident in both models, likely accommodating various tRNA substrates with thiouridine modifications.

For model 2 (with only S/Fe restraint), the RMSD of the catalytic domain is stable during the last 100 ns of the 260 ns simulation. The structure revisits catalytically relevant conformations, where the Ser113 hydroxyl hydrogen and Glu51 sidechain carboxy oxygen distances reach ∼2 Å throughout the simulation.

The amino acids Glu51, Ser111 and Ser113, previously identified as catalytic based on RudS homology with TudS, produced inactive enzymes when mutated to methionines (Figure 3C). The catalytic center geometries in model 1 and model 2 are illustrated in Figure 8. We identified an additional catalytic amino acid, Arg60, which functions to orient Glu51 (Figure 8B) and provide a positive charge that could stabilize transitional states during proton removal from water and the nucleophilic attack of thiouridine by the produced hydroxide ion. This arginine is fully conserved in the entire family of homologous proteins. Retrospective analysis revealed a homologous arginine serving the same purpose in the experimentally determined structure of TudS (60). Comparison of randomly selected frames from model 2 and model 1 molecular dynamics shows that the orientations of catalytic amino acids relative to the thiouridine moiety are very similar in both models (Figure 8C).

Both models feature an additional base involved in tRNA-enzyme active site binding (Figure 9A and B). In the experimental tRNA structure, the base U45 (PDBID: 6y3g) is unpaired and was initially dangling outside during tRNA simulations, whether the thiouridine side chain was paired inside or manually flipped outside. To our knowledge, a similar flipped uridine is present in at least three other known *E. coli* tRNA structures: valine tRNA (PDBID: 7eqj), initiator formylmethionine tRNA (PDBID: 5l4o), and aspartate tRNA (PDBID: 6ugg). This uridine participates in an extensive network, forming a double hydrogen bond with Asn26. The nearby Arg24 suggests the possibility of a cation-π stabilizing interaction, being oriented by a hydrogen bond with the backbone carbonyl oxygen atom of Gly27. These structural observations are consistent in both models. Mutating these amino acids to methionine results in diminished RudS_KT enzymatic desulfidase activity (Supplementary Figure S9). The somewhat smaller-than-anticipated change in enzymatic activity can be explained by methionine's ability to form hydrogen bonds. Additionally, mutating Tyr25 to methionine resulted in a mutant protein functionally identical to the wild type. We constructed two additional mutants: Tyr25 to alanine, which had decreased activity, and Tyr25 to phenylalanine, which had the same activity as the wild type (Supplementary Figure S9).

The DUF1722 domain in RudS_KT interacts with both the anticodon stem and the anticodon of tRNAs (Figure 10A).

Table 2. Effect of mutagenesis of predicted RudS_KT amino acids involved in enzymatic catalysis and/or substrate binding for s4U content in total *E. coli* tRNA

Mutant	AVG	stdev	*P*-value	Group	Remarks
WT	0.04	0	–	–	Wild type RudS_KT
E51M	1.06	0.06	****	CAT	Catalytic amino acid; conserved; removes proton from water molecule
S111M	0.98	0.13	****	CAT	Catalytic amino acid; conserved; stabilizes Glu51
S113M	0.86	0.08	****	CAT	Catalytic amino acid; stabilizes Glu51
R24M	0.14	0.02	**	G1	Interacts with Gly27 backbone carbonyl, Asn26 side chain carbonyl and nearby ribose ring oxygen. Pi-stacking interaction with U45
Y25M	0.07	0.03	n.s.	G1	Shields active center from the tRNAs phosphates. Opportunistically forms hydrogen bond with ribose OH group
Y25A	0.17	0.01	****	G1	
Y25F	0.04	0	n.s.	G1	
N26M	0.14	0.06	**	G1	Interacts with U45 forming hydrogen bond
G27M	0.16	0.01	***	G1	Part of flexible loop, forms hydrogen bond with Arg24 via backbone carbonyl
H29M	0.07	0	n.s.	G1	No important interactions observed
K30M	0.05	0.01	n.s.	G1	Occasionally interacts with tRNA phosphates and Asp33
D33M	0.04	0.01	n.s.	G1	No important interactions observed (salt bridge with Arg36)
R36M	0.05	0.02	n.s.	G1	No important interactions observed (salt bridge with Asp33)
K37M	0.06	0.03	n.s.	G1	No important interactions observed
R60M	0.89	0.11	****	G2	Catalytic amino acid; stabilizes Glu51
D61M	0.05	0.03	n.s.	G2	Occasionally interacts with bases in the tRNA
R64M	0.15	0.05	***	G2	Occasionally interacts with riboses in the tRNA
K110M	0.05	0.02	n.s.	G3	Interacts with thiouridine base ribose and phosphate in tRNA
E117M	0.06	0.02	n.s.	G3	Salt bridge with Arg155
R118M	0.09	0.01	n.s.	G3	Interaction with tRNAs riboses
K120M	0.1	0.01	n.s.	G3	Interaction with tRNAs phosphates
Y122M	0.1	0.01	n.s.	G3	Orientation of Lys120 and Arg64
H127M	0.04	0.01	n.s.	G3	No interaction
H131M	0.06	0.02	n.s.	G3	No interaction
K110M, K120M	0.28	0.05	****	G3	Synergistic effect, Lys110 partial compensation by Lys120
E152M	0.15	0.01	***	G4	Salt bridge with Arg155
R155M	0.24	0.02	****	G4	Salt bridge with Glu152, Van der Waals interaction with tRNA ribose
H157M	0.09	0	n.s.	G4	Hydrogen bond with ribose ring oxygen
N202M	0.21	0	****	G5	Backbone stabilization via side chain in turn
N203M	0.36	0.06	****	G5	Backbone stabilization via side chain in turn
Q205M	0.04	0.01	n.s.	G5	No interaction
R240M	0.06	0.02	n.s.	G6	No interaction
C241M	0.16	0.04	****	G6	No interaction
S243M	0.47	0.06	****	G6	Interaction with anticodon base
R244M	0.53	0.07	****	G6	Interaction with phosphate in anticodon region
T246M	0.18	0.02	****	G6	Backbone interaction via side chain; interaction with Ser243

AVG – relative s4U content, stdev – standard deviation. Statistical significance was calculated by applying one-way ANOVA with Dunnet's post-hoc test. $^{****}P < 0.0001$, $^{***}P < 0.001$, $^{**}P < 0.01$, n.s.: $P \geq 0.05$ compared to WT.

While the molecular dynamics simulations may not depict the final binding state accurately, specific frames identified highlight the significance of Ser243 and Arg244. Our hypothesis suggests that these amino acids, potentially along with other unidentified residues, interact with the anticodon bases and the anticodon phosphate backbone (Figure 10B,C, and D). These interactions are mostly opportunistic, except for Arg244, which predominantly interacts with tRNA backbone phosphates. A summary of the rationale behind the enzymatic activities of other mutants is outlined in Table 2. These models serve as explanatory tools for most of the experimentally observed desulfidase activities of the mutants, though they should be regarded as hypotheses rather than definitive structural representations.

Overexpression of RudS_KT in *E. coli* diminishes UVA-triggered growth delay

To gain insight into the potential role of RudS proteins in bacterial physiology, we overexpressed RudS_KT in *E. coli* and subjected the cells to UVA. Since 4-thiouridine is a known effector of bacterial UVA response, causing a growth delay and stringent response (97), we expected that the overexpression of RudS_KT could help overcome the previously reported UVA-induced growth delay in *E. coli* (98). The bacteria were exposed to approximately 100 kJ/m^2 UVA, and their growth was subsequently monitored. Control samples were kept in darkness. Both RudS_KT overexpressing and control samples kept in the dark (Figure 11, open symbols) did not show any notable difference at the initial growth stage, indicating that recombinant protein did not have a significant impact initially. However, differences began to appear after 3 h, with the growth of RudS_KT overexpressing bacteria (blue symbols) slowing down in comparison to empty vector-carrying bacteria (black symbols). UVA irradiation indeed slowed the growth of *E. coli* (Figure 11, solid symbols), causing a ∼105 min growth delay compared to non-irradiated empty vector-carrying cells. Remarkably, the overexpression of RudS_KT reduced this delay to approximately 60 minutes, indicating a positive effect on bacterial growth under these experimental conditions. The difference in the growth lag between irradiated RudS_KT overexpressing cells (blue symbols) and empty vector-carrying cells (black symbols) was approximately 45 min.

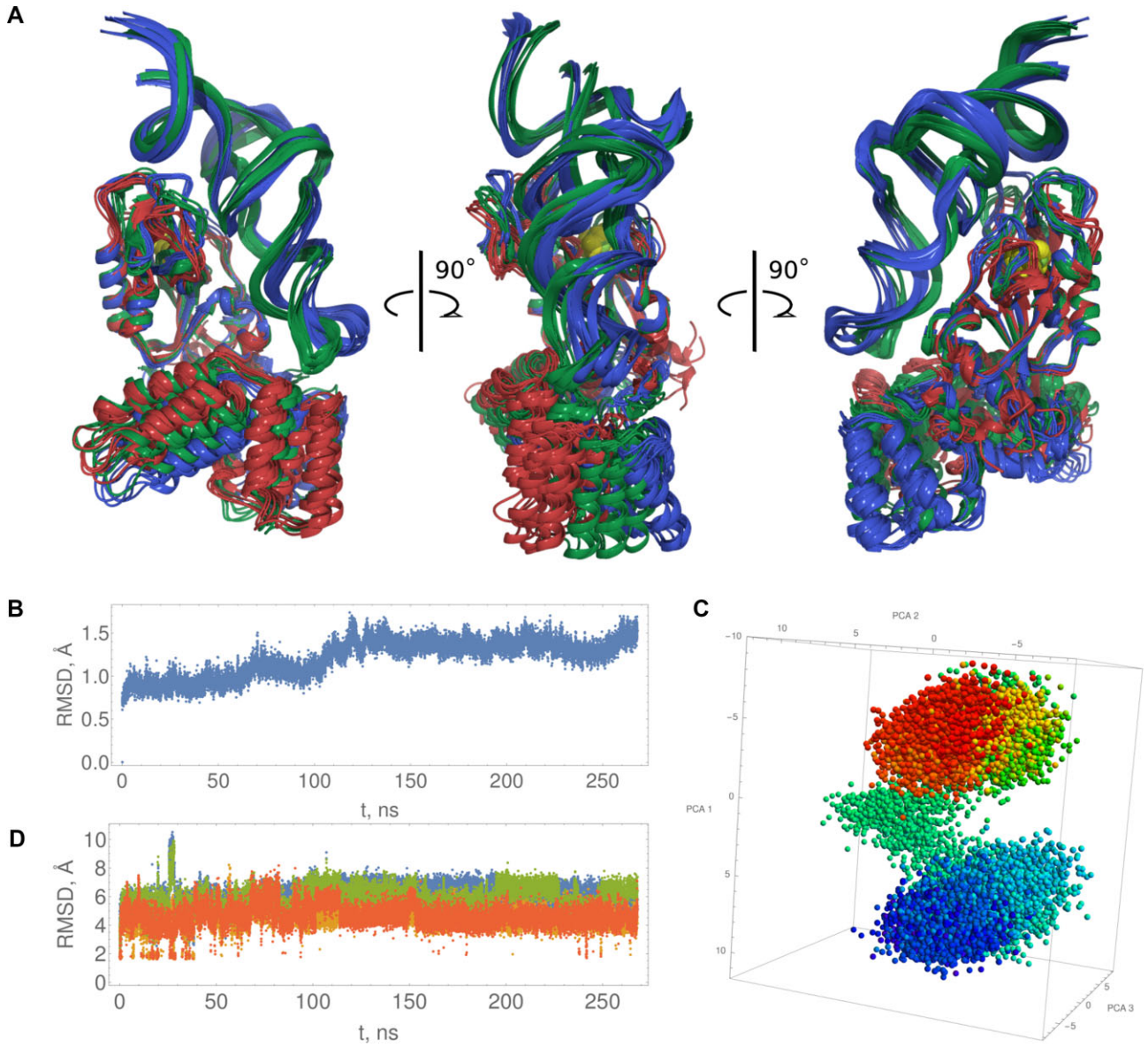

Figure 7. (**A**) Superposition of model 1 (blue), model 2 (green) and homoenzyme (red) final models. (**B**) Model 2 RMSD of the catalytic domain. (**C**) model 2 PCA of catalytic domain. (**D**) Red and orange Ser113 hydroxy hydrogen – Glu51 sidechain carboxy oxygen distances, green and blue Ser111 hydroxy hydrogen – Glu51 sidechain carboxy oxygen distances.

Discussion

While the understanding of TudS desulfidases is evolving, the function and structure of the Domain of Unknown Function 1722 have remained elusive until now. Previous studies from our group suggested that additional domains fused to TudS might influence its substrate preferences, potentially even accommodating intact tRNA molecules (39,40,58). This study successfully demonstrates that the DUF1722 domain facilitates the targeted removal of s4U modification from tRNA molecules by the RudS (TudS-DUF1722 fusion) proteins both *in vivo* and *in vitro*.

Structural insights and catalytic mechanism

Structural examination of RudS_KT from *Pseudomonas putida* KT2440 was conducted using molecular docking and molecular dynamics simulations, with subsequent experimental investigation connecting the proposed models and experimentally observed desulfidase activities of mutants. The investigation of the hypothesized catalytic amino acids (Glu51, Ser111, Ser113 and Arg60) and cysteines holding iron-sulfur cluster (Cys17, Cys49 and Cys114) by mutational analysis essentially abolished the RudS desulfidase activity, confirming their critical role in catalysis. Additionally, the models identified other important residues (Asn26, Arg24, Tyr25, Ser243, Arg244) for tRNA binding and catalysis, and their mutations resulted in diminished RudS_KT enzymatic activities. The effects of single amino acid substitutions to methionine (61) were all in line with the models we propose, except in the case of Tyr25, where two additional mutants were employed. The Tyr25 mutation to methionine was functionally identical to the WT enzyme, which is at odds with its position in the modeled complex—Tyr25 provides shielding of the active center from tRNA's phosphates and their negative charge, which would destabilize the transitional state and disrupt catalysis. The RudS_KT Tyr25 to alanine mutant displayed decreased

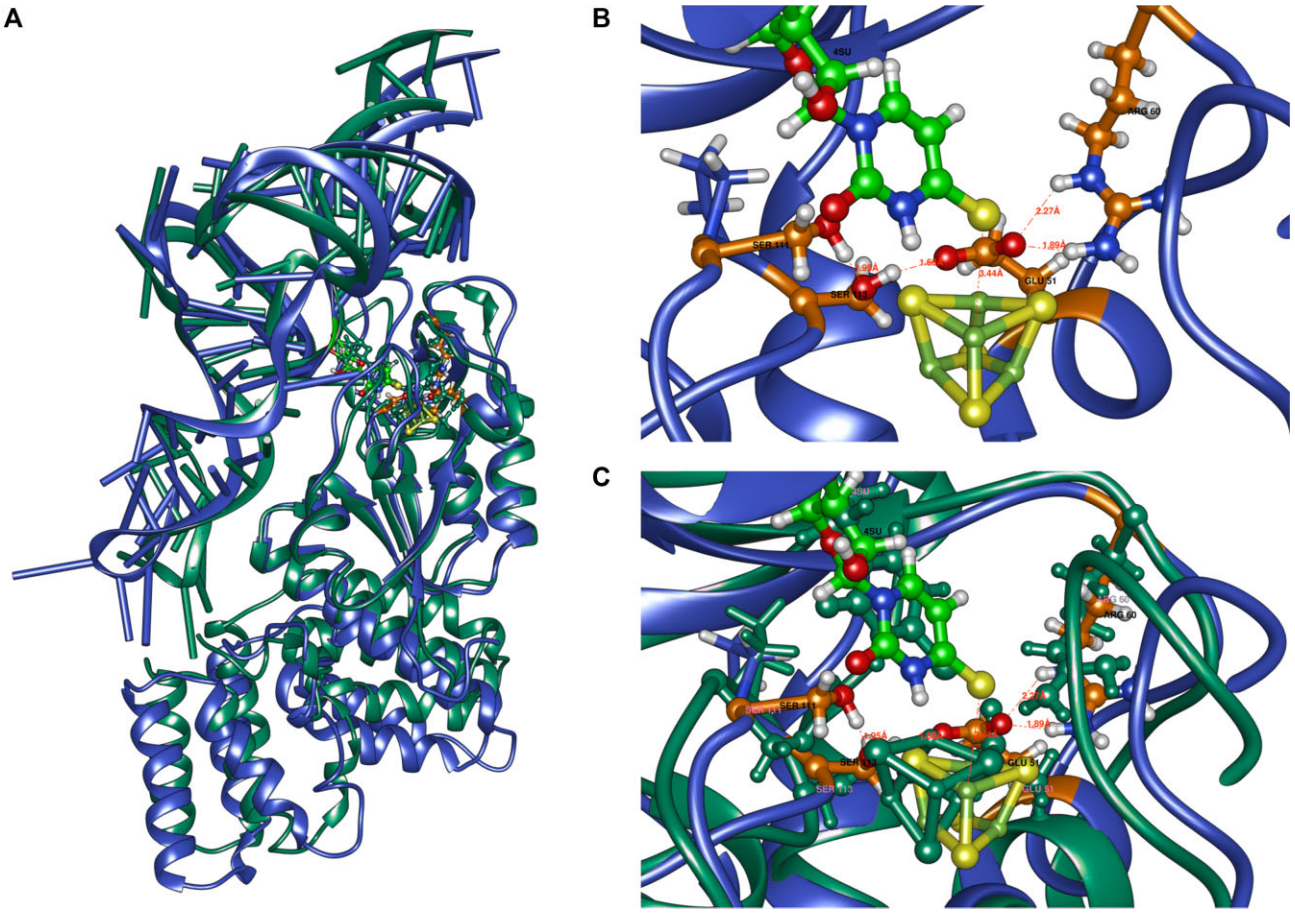

Figure 8. (**A**) overall superposition of model1 (blue, the S/Fe restraint and additional restraints on catalytic distances) and model 2 (pink, only the S/Fe restraint). (**B**) catalytic center with relevant distances indicated. (**C**) superposition of catalytic centers of model 1 and model 2.

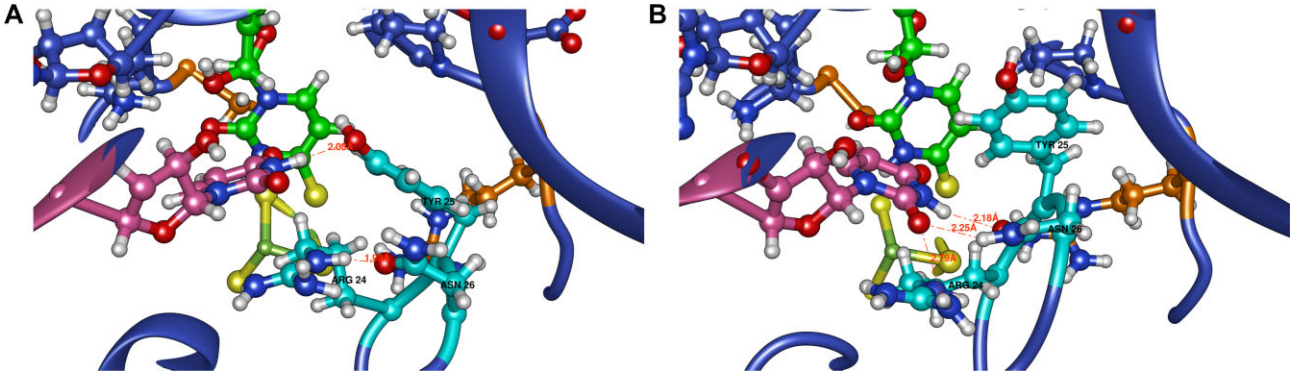

Figure 9. (**A** and **B**) U45 (pink) interactions with Arg24, Tyr25, Asn26 (cyan), and thiouridine (green).

enzymatic activity, while the Tyr25 to phenylalanine mutant retained the same activity as WT. We propose that methionine is large enough to provide substantial electrostatic shielding; therefore, only the Tyr25 to alanine variant function was significantly affected by the substitution.

The proposed models of the RudS enzyme–tRNA substrate complex suggest that the DUF1722 domain primarily interacts with the anticodon arm and anticodon of the tRNA substrate, while the catalytic TudS domain interacts with the variable loop, acceptor stem, and D arm of the tRNA. Moreover, the elongated loops encompassing amino acids 116–135 and 18–33, along with the mobility of the DUF1722 domain, likely aid in the recognition and adaptation of a diverse array of tRNAs containing the 4-thiouridine modification at position 8. This functional specialization between the two domains likely enables the precise elimination of the s4U modification from the tRNA molecule by RudS.

Evolutionary insights and functional implications

The DUF1722 genes are predominantly reported in bacteria (94.2% of all sequences) with archaeal DUF1722 making up only 5.1%. 74.4% of DUF1722s are fused with the TudS gene and only 21.4% of known DUF1722 genes encode a stand-

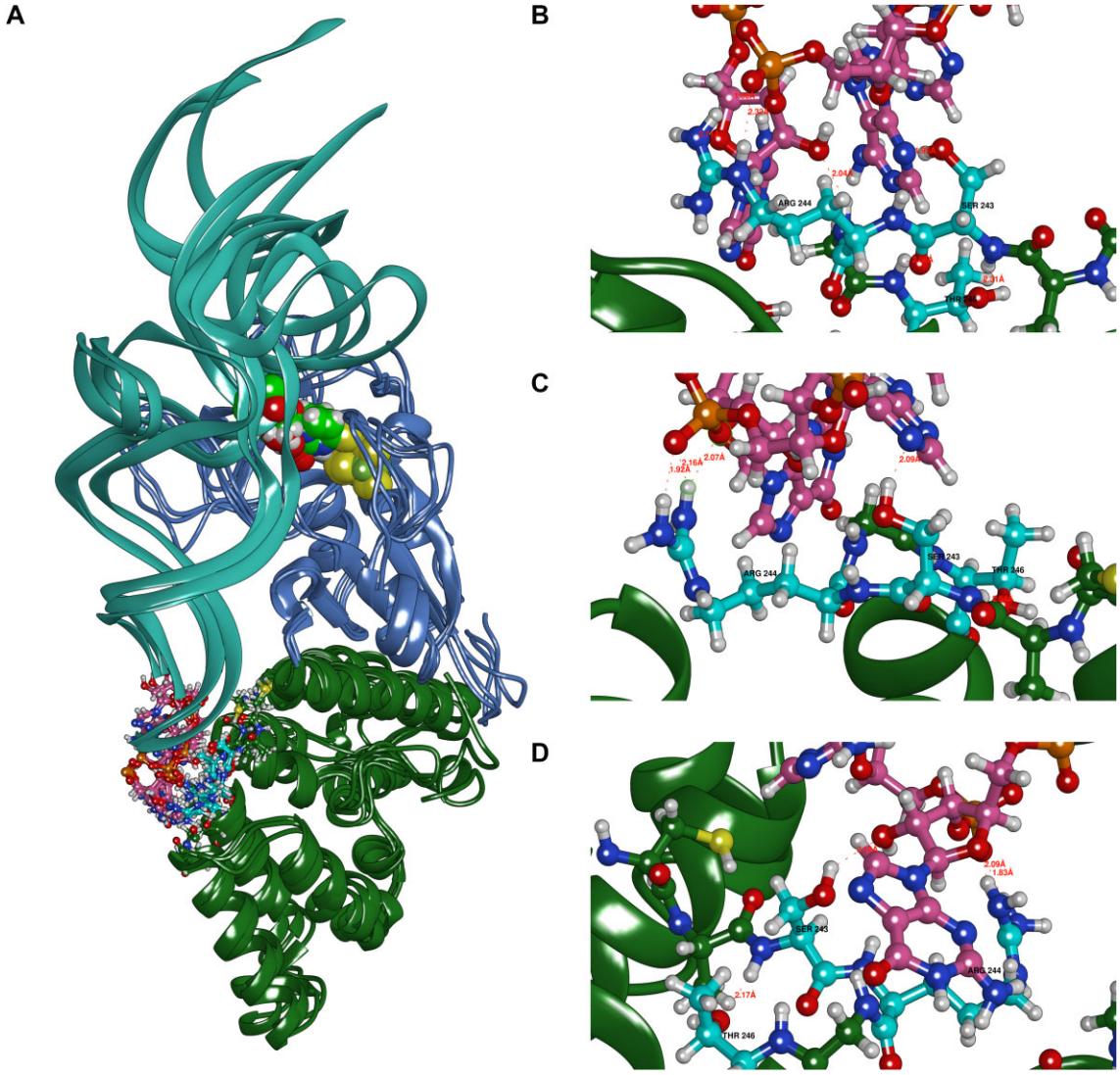

Figure 10. (**A**) Overall structure of the complex. Spheres represent 4-thiouridine and the iron-sulfur cluster. The DUF1722 domain is shown in dark green. The anticodon part of the tRNA is depicted with explicit pink ball-and-stick atom representations. (**B–D**) Various conformations of Ser243 and Arg244 interacting with tRNA and Thr246 (amino acids in cyan).

alone protein (86). Genes encoding RudS are often found in light-responsive operons (Supplementary Figure S10), which are responsible for UV-induced DNA damage repair (i.e., DNA-photolyases) or light-induced oxidative stress response (i.e., carotenoid biosynthesis gene clusters) (99). Recent studies in the genus *Pseudomonas* have revealed the role of light-inducible transcriptional regulators in controlling the expression of light-responsive genes. These regulators belong to the MerR family and are adenosyl B12-dependent, making them sensitive to light (class II LitR regulators). In the dark, LitR regulators function as negative regulators, suppressing the transcription of light-inducible genes. However, when exposed to 450 nm blue light, LitRs become deactivated. One of the operons controlled by this mechanism encodes PhrB DNA photolyase, LitR, and RudS (100,101).

At the same time, the tRNA s4U modification is known to act as a photosensitive residue in tRNA, crosslinking with neighboring cytidine in the 13th position upon exposure to near-UV radiation. Near-UV light triggers a bacterial growth delay effect causing some tRNA species to become poor substrates for aminoacylation resulting in accumulation of uncharged tRNA and transient cessation of protein synthesis (30,102). The accumulation of ribosomes stalled with non-aminoacylated tRNA is known to initiate a stringent response (103), which is the most likely mechanism causing alarmone guanosine tetraphosphate (ppGpp) accumulation after cell irradiation by UV-A (98,104).

Paradoxically, *E. coli* Δ*thiI* mutants, incapable of s4U tRNA modification biosynthesis, are less susceptible to the combination of short wavelength UV and UVA, as s4U is the primary target of latter irradiation. Subsequently, this eliminates a damaging synergistic effect of UVA and UVB or UVC irradiation observed in *E. coli* (105,106). The presence of RudS gene in such cases could help overcome UVA-induced deceleration of protein synthesis, thereby ensuring the functionality of DNA damage repair machinery. On the other hand, studies with *Salmonella typhimurium* revealed that 4-thiouridine plays a crucial role in resistance to near-UV irradiation, with mutants lacking 4-thiouridine and those deficient in ppGpp synthesis being sensitive to near-UV-induced killing;

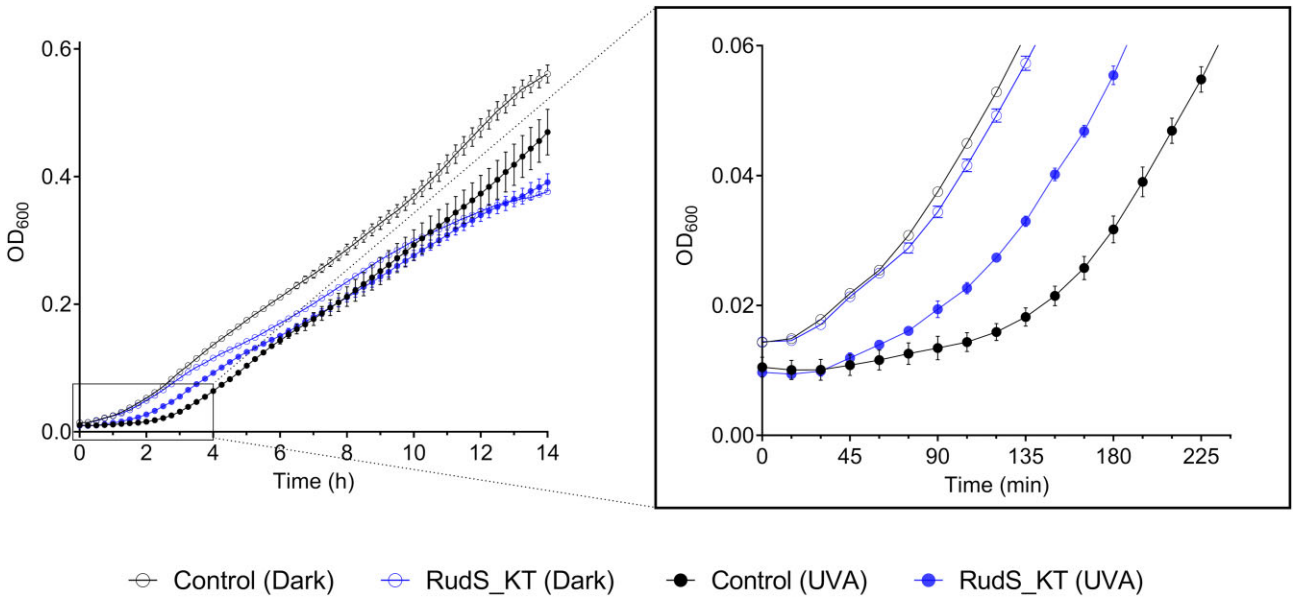

Figure 11. UVA-triggered growth delay reduction in *E. coli* BL21(DE3) overexpressing RudS_KT. Solid symbols represent the growth curves of UVA-irradiated bacteria overexpressing RudS_KT (blue symbols) and carrying empty vector (black symbols). Open symbols represent the growth curves of RudS_KT overexpressing bacteria (blue symbols) and bacteria carrying the empty vector (black symbols) maintained in the dark within the same period.

it further suggested a model wherein ppGpp and ApppGpp induce the synthesis of a set of then unidentified proteins essential for resistance to near-UV irradiation in response to the cross-linking of 4-thiouridine in tRNA (104). It is worth noting that *Salmonella typhimurium* possesses a RudS encoding gene (RudS_ST in this study, ORF319 previously) under the control of a transcription regulator of MerR family (88,107), while *E. coli* does not.

The prevalence of DUF1722 genes in bacteria, often fused with TudS, and their association with light-responsive genes, suggest a light-induced mechanism for prokaryotic tRNA s4U de-modification. This mechanism may play a role in regulating alarmone levels during UV-induced tRNA cross-linking and the stringent response, serving as a bacterial survival strategy under UV stress. Although in vitro experiments showed no changes in the enzymatic activity of RudS_KT in the presence of the (p)ppGpp molecules, this does not rule out the possibility that the alarmones and RudS are part of the same regulatory mechanism within the cell, interacting through currently unknown intermediary factors or pathways.

This hypothesis is further supported by the case of *Enterobacter cloacae*, which demonstrated that pre-treating bacteria with sub-lethal doses of UVA radiation activates an unidentified mechanism, leading to a reduction in the 4-thiouridine content of tRNA that helps to evade the growth delay caused by crosslinked tRNA during subsequent UVA irradiation (108). In the genome sequence of *E. cloacae* (GenBank: CP135498.1), the RudS encoding gene (locus tag: RRL13_00330) is in the immediate vicinity to the MerR family transcriptional regulator (locus tag: RRL13_00340), suggesting a light-inducible RudS gene expression, which might explain the observed effect. Furthermore, a previous study by the same authors revealed that after the exposure to UVA, not only a growth delay was induced in both *E. cloacae* and *E. coli*, but also a burst of ppGpp was observed (98). However, the ppGpp amounts accumulated in *E. coli* were twice those reached in *E. cloacae*. Moreover, the time needed to restore ppGpp content to basal levels in *E. cloacae* was shorter than that required in *E. coli*. This period aligned with the time when growth resumed at its normal rate in both species. It should be pointed out that *E. coli* genome encodes a stand-alone DUF1722 domain YbgA, while *E. cloacae* encodes a RudS fusion protein. Both these species lack a stand-alone TudS. We speculate that *E. cloacae*, which possesses a RudS fusion protein, was able to reduce the 4-thiouridine content of tRNA and mitigate the growth delay caused by cross-linked tRNA during UVA irradiation. In contrast, the *E. coli*, which lacks a stand-alone RudS and instead encodes a stand-alone DUF1722 domain (YbgA), exhibited a more pronounced stringent response and delayed recovery after UVA exposure. As indicated by our observations, the temporary *E. coli* growth arrest following UVA-stress can be substantially lessened in the presence of RudS (Figure 11). These observations confirm that the function of RudS is different from that of a stand-alone DUF1722 and that of a stand-alone TudS. There is a possibility that during evolution, in certain species, the gene encoding RudS may have undergone a split, resulting in separate stand-alone TudS and stand-alone DUF1722 encoding genes.

Moreover, nano-tRNAseq analysis of tRNA extracted from RudS_KT overexpressing *E. coli* cells revealed a significant decrease (~2-fold) in the abundance of $tRNA^{Ser(GTC)}$ and $tRNA^{Tyr(GTA)}$ compared to control samples (Supplementary Figure S11). These findings parallel previous observations (22) that the lack of s4U modification causes a degradosome-mediated degradation of $tRNA^{Ser(TGA)}$ and $tRNA^{Tyr(GTA)}$ in *Vibrio cholerae* during the stationary growth phase. Although the reduction we observed in *E. coli* is not as dramatic as in *Vibrio cholerae*, this co-occurrence suggests an underlying physiological mechanism that responds to s4U levels in tRNA.

Conclusions

This study provides compelling evidence that RudS enzymes, consisting of a DUF1722 domain fused with the TudS desulfidase, facilitate the targeted removal of the s4U modification from tRNA molecules. We may speculate that certain bacterial species have evolved a light-inducible mechanism for tRNA s4U de-modification, which likely plays a role in regulating alarmone levels during a tRNA UV-crosslinking-induced stringent response-like state. By diminishing the available pool of tRNA substrate, such an adaptive process might mitigate continuous cross-linking, thereby preventing translation derangement. Such strategic adjustment may serve as a survival mechanism for bacteria, particularly in the face of intense UV radiation exposure, ensuring the seamless operation of stress-response machinery.

Data availability

The models are available in ModelArchive at https://www.modelarchive.org/doi/10.5452/ma-6xegk.

Supplementary data

Supplementary Data are available at NAR Online.

Acknowledgements

The graphical abstract was created with BioRender.com.

We thank Justas Vaitekūnas for technical assistance.

Author contributions: R.J.: Formal analysis, Investigation, Methodology, Validation, Visualization, Writing – original draft, Writing – review & editing. A.L.: Formal analysis, Methodology, Validation, Visualization, Writing – original draft, Writing – review & editing. D.P.: Investigation, Validation, Writing – review & editing. R.M.: Conceptualization, Funding acquisition, Resources, Writing – review & editing. A.A.: Conceptualization, Formal analysis, Investigation, Validation, Supervision, Visualization, Writing – original draft, Writing – review & editing.

Funding

European Regional Development Fund under grant agreement with the Research Council of Lithuania (LMTLT) [01.2.2-LMT-K-718-03-0082 to R.M. and P-MIP-24-349 to A.A.]. Funding for open access charge: Lithuanian Research Library Consortium (LMBA).

Conflict of interest statement

None declared.

References

1. Shigi,N. (2014) Biosynthesis and functions of sulfur modifications in tRNA. *Front. Genet.*, **5**, 67.
2. Shigi,N. (2018) Recent advances in our understanding of the biosynthesis of sulfur modifications in tRNAs. *Front. Microbiol.*, **9**, 2679.
3. Čavužić,M. and Liu,Y. (2017) Biosynthesis of sulfur-containing tRNA modifications: a comparison of bacterial, archaeal, and eukaryotic pathways. *Biomolecules*, **7**, 27.
4. Zheng,C., Black,K.A. and Dos Santos,P.C. (2017) Diverse mechanisms of sulfur decoration in bacterial tRNA and their cellular functions. *Biomolecules*, **7**, 33.
5. Rozenski,J., Crain,P.F. and McCloskey,J.A. (1999) The RNA modification database: 1999 update. *Nucleic Acids Res.*, **27**, 196–197.
6. Laxman,S., Sutter,B.M., Wu,X., Kumar,S., Guo,X., Trudgian,D.C., Mirzaei,H. and Tu,B.P. (2013) Sulfur amino acids regulate translational capacity and metabolic homeostasis through modulation of tRNA thiolation. *Cell*, **154**, 416.
7. Gupta,R., Walvekar,A.S., Liang,S., Rashida,Z., Shah,P. and Laxman,S. (2019) A tRNA modification balances carbon and nitrogen metabolism by regulating phosphate homeostasis. *Elife*, **8**, e44795.
8. Murphy,F. V., Ramakrishnan,V., Malkiewicz,A. and Agris,P.F. (2004) The role of modifications in codon discrimination by tRNALysUUU. *Nat. Struct. Mol. Biol.*, **11**, 1186–1191.
9. Shigi,N. (2021) Biosynthesis and degradation of sulfur modifications in tRNAs. *Int. J. Mol. Sci.*, **22**, 11937.
10. Agris,P.F., Sierzputowska-Gracz,H., Smith,W., Malkiewicz,A., Sochacka,E. and Nawrot,B. (1992) Thiolation of uridine carbon-2 restricts the motional dynamics of the transfer RNA wobble position nucleoside. *J. Am. Chem. Soc.*, **114**, 2652–2656.
11. Yokoyama,S., Watanabe,T., Murao,K., Ishikura,H., Yamaizumi,Z., Nishimura,S. and Miyazawa,T. (1985) Molecular mechanism of codon recognition by tRNA species with modified uridine in the first position of the anticodon. *Proc. Natl. Acad. Sci. U.S.A.*, **82**, 4905–4909.
12. Agris,P.F., Soil,D. and Seno,T. (1973) Biological function of 2-thiouridine in Escherichia coli glutamic acid transfer ribonucleic acid. *Biochemistry*, **12**, 4331–4337.
13. Jenner,L.B., Demeshkina,N., Yusupova,G. and Yusupov,M. (2010) Structural aspects of messenger RNA reading frame maintenance by the ribosome. *Nat. Struct. Mol. Biol.*, **17**, 555–560.
14. Johansson,M.J.O., Esberg,A., Huang,B., Björk,G.R. and Byström,A.S. (2008) Eukaryotic wobble uridine modifications promote a functionally redundant decoding system. *Mol. Cell. Biol.*, **28**, 3301–3312.
15. Shigi,N., Sakaguchi,Y., Suzuki,T. and Watanabe,K. (2006) Identification of two tRNA thiolation genes required for cell growth at extremely high temperatures. *J. Biol. Chem.*, **281**, 14296–14306.
16. Rose,S., Auxilien,S., Havelund,J.F., Kirpekar,F., Huber,H., Grosjean,H. and Douthwaite,S. (2020) The hyperthermophilic partners Nanoarchaeum and Ignicoccus stabilize their tRNA T-loops via different but structurally equivalent modifications. *Nucleic Acids Res.*, **48**, 6906–6918.
17. Durant,P.C., Bajji,A.C., Sundaram,M., Kumar,R.K. and Davis,D.R. (2005) Structural effects of hypermodified nucleosides in the Escherichia coli and human tRNALys anticodon loop: the effect of nucleosides s 2U, mcm5U, mcm5s2U, mnm 5s2U, t6A, and ms2t6A. *Biochemistry*, **44**, 8078–8089.
18. Jäger,G., Leipuviene,R., Pollard,M.G., Qian,Q. and Björk,G.R. (2004) The conserved Cys-X1-X2-Cys motif present in the TtcA protein is required for the thiolation of cytidine in position 32 of tRNA from Salmonella enterica serovar Typhimurium. *J. Bacteriol.*, **186**, 750–757.
19. Sochacka,E., Bartos,P., Kraszewska,K. and Nawrot,B. (2013) Desulfuration of 2-thiouridine with hydrogen peroxide in the physiological pH range 6.6-7.6 is pH-dependent and results in two distinct products. *Bioorg. Med. Chem. Lett.*, **23**, 5803–5805.
20. Cappannini,A., Ray,A., Purta,E., Mukherjee,S., Boccaletto,P., Moafinejad,S.N., Lechner,A., Barchet,C., Klaholz,B.P., Stefaniak,F., *et al.* (2023) MODOMICS: a database of RNA modifications and related information. *Nucleic Acids Res*, **52**, D239–D244.
21. Tomikawa,C., Ohira,T., Inoue,Y., Kawamura,T., Yamagishi,A., Suzuki,T. and Hori,H. (2013) Distinct tRNA modifications in the

thermo-acidophilic archaeon, Thermoplasma acidophilum. *FEBS Lett.*, **587**, 3575–3580.
22. Kimura,S. and Waldor,M.K. (2019) The RNA degradosome promotes tRNA quality control through clearance of hypomodified tRNA. *Proc. Natl. Acad. Sci. U.S.A.*, **116**, 1394–1403.
23. Griffey,R.H., Davis,D.R. and Yamaizumi,Z. (1986) 15N-labeled tRNA. Identification of 4-thiouridine in Escherichia coli tRNA1(Ser) and tRNA2(Tyr) by 1H-15N two-dimensional NMR spectroscopy. *J. Biol. Chem.*, **261**, 12074–12078.
24. Mueller,E.G., Buck,C.J., Palenchar,P.M., Barnhart,L.E. and Paulson,J.L. (1998) Identification of a gene involved in the generation of 4-thiouridine in tRNA. *Nucleic Acids Res.*, **26**, 2606–2610.
25. He,N., Zhou,J., Bimai,O., Oltmanns,J., Ravanat,J.L., Velours,C., Schünemann,V., Fontecave,M. and Golinelli-Pimpaneau,B. (2022) A subclass of archaeal U8-tRNA sulfurases requires a [4Fe-4S] cluster for catalysis. *Nucleic Acids Res.*, **50**, 12969–12978.
26. Martinez-Gomez,N.C., Palmer,L.D., Vivas,E., Roach,P.L. and Downs,D.M. (2011) The rhodanese domain of ThiI is both necessary and sufficient for synthesis of the Thiazole moiety of thiamine in Salmonella enterica. *J. Bacteriol.*, **193**, 4582–4587.
27. Rajakovich,L.J., Tomlinson,J. and Dos Santos,P.C. (2012) Functional analysis of Bacillus subtilis genes involved in the biosynthesis of 4-thiouridine in tRNA. *J. Bacteriol.*, **194**, 4933–4940.
28. Hori,H. (2023) Transfer RNA modification enzymes with a thiouridine synthetase, methyltransferase and pseudouridine synthase (THUMP) domain and the nucleosides they produce in tRNA. *Genes (Basel)*, **14**, 382.
29. Lorenz,C., Lünse,C.E. and Mörl,M. (2017) tRNA modifications: impact on structure and thermal adaptation. *Biomolecules*, **7**.
30. Carre,D.S., Thomas,G. and Favre,A. (1974) Conformation and functioning of tRNAs: cross-linked tRNAs as substrate for tRNA nucleotidyl-transferase and aminoacyl synthetases. *Biochimie*, **56**, 1089–1101.
31. Nomura,Y., Ohno,S., Nishikawa,K. and Yokogawa,T. (2016) Correlation between the stability of tRNA tertiary structure and the catalytic efficiency of a tRNA-modifying enzyme, archaeal tRNA-guanine transglycosylase. *Genes to Cells*, **21**, 41–52.
32. Hori,H., Saneyoshi,M., Kumagai,I., Miura,K.I. and Watanabe,K. (1989) Effects of modification of 4-thiouridine in E. coli tRNA(fMet) on its methyl acceptor activity by thermostable Gm-methylases. *J. Biochem.*, **106**, 798–802.
33. Li,Z., Reimers,S., Pandit,S. and Deutscher,M.P. (2002) RNA quality control: degradation of defective transfer RNA. *EMBO J.*, **21**, 1132–1138.
34. Davis,B.D., Luger,S.M. and Tai,P.C. (1986) Role of ribosome degradation in the death of starved Escherichia coli cells. *J. Bacteriol.*, **166**, 439–445.
35. Svenningsen,S. Lo, Kongstad,M., Stenum,T.S., Muñoz-Gómez,A.J. and Sørensen,M.A. (2017) Transfer RNA is highly unstable during early amino acid starvation in Escherichia coli. *Nucleic Acids Res.*, **45**, 793–804.
36. Preumont,A., Snoussi,K., Stroobant,V., Collet,J.F. and Van Schaftingen,E. (2008) Molecular identification of pseudouridine-metabolizing enzymes. *J. Biol. Chem.*, **283**, 25238–25246.
37. Hitchcock,D.S., Fedorov,A.A., Fedorov,E. V., Almo,S.C. and Raushel,F.M. (2014) Discovery of a bacterial 5-methylcytosine deaminase. *Biochemistry*, **53**, 7426–7435.
38. Mitsukawa,Y., Hibi,M., Matsutani,N., Horinouchi,N., Takahashi,S. and Ogawa,J. (2016) A novel nucleoside hydrolase from lactobacillus buchneri LBK78 catalyzing hydrolysis of 2′-O-methylribonucleosides. *Biosci. Biotechnol. Biochem.*, **80**, 1568–1576.
39. Aučynaitė,A., Rutkienė,R., Gasparavičiūtė,R., Meškys,R. and Urbonavičius,J. (2018) A gene encoding a DUF523 domain protein is involved in the conversion of 2-thiouracil into uracil. *Environ. Microbiol. Rep.*, **10**, 49–56.
40. Fuchs,J., Jamontas,R., Hoock,M.H., Oltmanns,J., Golinelli-Pimpaneau,B., Schünemann,V., Pierik,A.J., Meškys,R., Aučynaitė,A. and Boll,M. (2023) TudS desulfidases recycle 4-thiouridine-5’-monophosphate at a catalytic [4Fe-4S] cluster. *Commun. Biol.*, **6**, 1092.
41. Aučynaite,A., Rutkiene,R., Tauraite,D., Meškys,R. and Urbonavičius,J. (2018) Discovery of bacterial deaminases that convert 5-fluoroisocytosine into 5-fluorouracil. *Front. Microbiol.*, **9**, 2375.
42. Stanislauskienė,R., Laurynėnas,A., Rutkienė,R., Aučynaitė,A., Tauraitė,D., Meškienė,R., Urbelienė,N., Kaupinis,A., Valius,M., Kaliniene,L., *et al.* (2020) YqfB protein from Escherichia coli: an atypical amidohydrolase active towards N 4-acylcytosine derivatives. *Sci. Rep.*, **10**, 788.
43. Aučynaite,A., Rutkiene,R., Tauraite,D., Meškys,R. and Urbonavičius,J. (2018) Identification of a 2’-O-methyluridine nucleoside hydrolase using the metagenomic libraries. *Molecules*, **23**, 2904.
44. Kimura,S., Srisuknimit,V., McCarty,K.L., Dedon,P.C., Kranzusch,P.J. and Waldor,M.K. (2022) Sequential action of a tRNA base editor in conversion of cytidine to pseudouridine. *Nat. Commun.*, **13**, 59–94.
45. Wei,J., Liu,F., Lu,Z., Fei,Q., Ai,Y., He,P.C., Shi,H., Cui,X., Su,R., Klungland,A., *et al.* (2018) Differential m6A, m6Am, and m1A demethylation mediated by FTO in the cell nucleus and cytoplasm. *Mol. Cell*, **71**, 973–985.
46. Liu,F., Clark,W., Luo,G., Wang,X., Fu,Y., Wei,J., Wang,X., Hao,Z., Dai,Q., Zheng,G., *et al.* (2016) ALKBH1-mediated tRNA demethylation regulates translation. *Cell*, **167**, 816–828.
47. Arragain,S., Bimai,O., Legrand,P., Caillat,S., Ravanat,J.L., Touati,N., Binet,L., Atta,M., Fontecave,M., Golinelli-Pimpaneau,B., *et al.* (2017) Nonredox thiolation in tRNA occurring via sulfur activation by a [4Fe-4S] cluster. *Proc. Natl. Acad. Sci. U.S.A.*, **114**, 7355–7360.
48. Chen,M., Asai,S.I., Narai,S., Nambu,S., Omura,N., Sakaguchi,Y., Suzuki,T., Ikeda-Saito,M., Watanabe,K., Yao,M., *et al.* (2017) Biochemical and structural characterization of oxygen-sensitive 2-thiouridine synthesis catalyzed by an iron-sulfur protein TtuA. *Proc. Natl. Acad. Sci. U.S.A.*, **114**, 4954–4959.
49. Chen,M., Ishizaka,M., Narai,S., Horitani,M., Shigi,N., Yao,M. and Tanaka,Y. (2020) The [4Fe-4S] cluster of sulfurtransferase TtuA desulfurizes TtuB during tRNA modification in Thermus thermophilus. *Commun. Biol.*, **3**, 2–4.
50. Zhou,J., Lénon,M., Ravanat,J.L., Touati,N., Velours,C., Podskoczyj,K., Leszczynska,G., Fontecave,M., Barras,F. and Golinelli-Pimpaneau,B. (2021) Iron-sulfur biology invades tRNA modification: the case of U34 sulfuration. *Nucleic Acids Res.*, **49**, 3997–4007.
51. Bimai,O., Arragain,S. and Golinelli-Pimpaneau,B. (2020) Structure-based mechanistic insights into catalysis by tRNA thiolation enzymes. *Curr. Opin. Struct. Biol.*, **65**, 69–78.
52. Shigi,N., Horitani,M., Miyauchi,K., Suzuki,T. and Kuroki,M. (2020) An ancient type of MnmA protein is an iron-sulfur cluster-dependent sulfurtransferase for tRNA anticodons. *RNA*, **26**, 240–250.
53. Fugate,C.J. and Jarrett,J.T. (2012) Biotin synthase: Insights into radical-mediated carbon-sulfur bond formation. *Biochim. Biophys. Acta - Proteins Proteomics*, **1824**, 1213–1222.
54. McLaughlin,M.I., Lanz,N.D., Goldman,P.J., Lee,K.H., Booker,S.J. and Drennan,C.L. (2016) Crystallographic snapshots of sulfur insertion by lipoyl synthase. *Proc. Natl. Acad. Sci. U.S.A.*, **113**, 9446–9450.
55. McCarthy,E.L. and Booker,S.J. (2017) Destruction and reformation of an iron-sulfur cluster during catalysis by lipoyl synthase. *Science.*, **358**, 373–377.
56. McCarthy,E.L., Rankin,A.N., Dill,Z.R. and Booker,S.J. (2019) The A-type domain in Escherichia coli NfuA is required for

regenerating the auxiliary [4Fe–4S] cluster in Escherichia coli lipoyl synthase. *J. Biol. Chem.*, **294**, 1609–1617.
57. Bouvier,D., Labessan,N., Clémancey,M., Latour,J.M., Ravanat,J.L., Fontecave,M. and Atta,M. (2014) TtcA a new tRNA-thioltransferase with an Fe-S cluster. *Nucleic Acids Res.*, **42**, 7960–7970.
58. Zhou,J., Pecqueur,L., Aučynaitė,A., Fuchs,J., Rutkienė,R., Vaitekūnas,J., Meškys,R., Boll,M., Fontecave,M., Urbonavičius,J., *et al.* (2021) Structural evidence for a [4Fe-5S] intermediate in the non-redox desulfuration of thiouracil. *Angew. Chem. Int. Ed.*, **60**, 424–431.
59. Sambrook,J. and Russell,D.W. (2001) In: *Molecular Cloning: A Laboratory Manual*. Cold Spring Harb. Lab. Press, NY.
60. Huang,Y. and Zhang,L. (2017) An in vitro single-primer site-directed mutagenesis method for use in biotechnology. In: *Methods in Molecular Biology*. Humana Press Inc., Vol. **1498**, pp. 375–383.
61. Gray,V.E., Hause,R.J. and Fowler,D.M. (2017) Analysis of large-scale mutagenesis data to assess the impact of single amino acid substitutions. *Genetics*, **207**, 53–61.
62. Studier,F.W. (2005) Protein production by auto-induction in high density shaking cultures. *Protein Expr. Purif.*, **41**, 207–234.
63. The UniProt Consortium (2023) UniProt: the Universal Protein Knowledgebase in 2023. *Nucleic Acids Res.* **51**, 523–531.
64. Finn,R.D., Clements,J. and Eddy,S.R. (2011) HMMER web server: interactive sequence similarity searching. **39**, W29–W37.
65. Zimmermann,L., Stephens,A., Nam,S.Z., Rau,D., Kübler,J., Lozajic,M., Gabler,F., Söding,J., Lupas,A.N. and Alva,V. (2018) A Completely Reimplemented MPI Bioinformatics Toolkit with a New HHpred Server at its Core. *J. Mol. Biol.*, **430**, 2237–2243.
66. Cock,P.J.A., Antao,T., Chang,J.T., Chapman,B.A., Cox,C.J., Dalke,A., Friedberg,I., Hamelryck,T., Kauff,F., Wilczynski,B., *et al.* (2009) Biopython: freely available Python tools for computational molecular biology and bioinformatics. *Bioinformatics*, **25**, 1422–1423.
67. Sokal,R.R. and Michener,C.D. (1958) A statistical method for evaluating systematic relationships. **38**, 1409–1438.
68. Huerta-Cepas,J., Serra,F. and Bork,P. (2016) ETE 3: reconstruction, analysis, and visualization of phylogenomic data. *Mol. Biol. Evol.*, **33**, 1635–1638.
69. Catala,M., Gato,A., Tisné,C. and Barraud,P. (2020) Preparation of yeast tRNA sample for NMR spectroscopy. *Bio-protocol*, **10**, e3646.
70. Lucas,M.C., Pryszcz,L.P., Medina,R., Milenkovic,I., Camacho,N., Marchand,V., Motorin,Y., Ribas de Pouplana,L. and Novoa,E.M. (2024) Quantitative analysis of tRNA abundance and modifications by nanopore RNA sequencing. *Nat. Biotechnol.*, **42**, 72–86.
71. Edwards,A.M., Addo,M.A. and Dos Santos,P.C. (2021) tRNA modifications as a readout of S and Fe-S metabolism. *Methods Mol. Biol.*, **2353**, 137–154.
72. Hennessy,D.J., Reid,G.R., Smith,F.E. and Thompson,S.L. (1984) Ferene — a new spectrophotometric reagent for iron. *Can. J. Chem.*, **62**, 721–724.
73. Fernández,F.J., Gómez,S., Navas-Yuste,S., López-Estepa,M. and Vega,M.C. (2017) Protein-tRNA agarose gel retardation assays for the analysis of the N6-threonylcarbamoyladenosine TcdA function. *J. Vis. Exp.*, **2017**, 55638.
74. Bryant,P., Pozzati,G. and Elofsson,A. (2022) Improved prediction of protein-protein interactions using AlphaFold2. *Nat. Commun.*, **13**, 1265.
75. Du,Z., Su,H., Wang,W., Ye,L., Wei,H., Peng,Z., Anishchenko,I., Baker,D. and Yang,J. (2021) The trRosetta server for fast and accurate protein structure prediction. *Nat. Protoc.*, **16**, 5634–5651.
76. Steinegger,M. and Söding,J. (2017) MMseqs2 enables sensitive protein sequence searching for the analysis of massive data sets. *Nat. Biotechnol.*, **35**, 1026–1028.
77. Remmert,M., Biegert,A., Hauser,A. and Söding,J. (2012) HHblits: lightning-fast iterative protein sequence searching by HMM-HMM alignment. *Nat. Methods*, **9**, 173–175.
78. Lee,T.S., Allen,B.K., Giese,T.J., Guo,Z., Li,P., Lin,C., Dwight McGee,T., Pearlman,D.A., Radak,B.K., Tao,Y., *et al.* (2020) Alchemical binding free energy calculations in AMBER20: advances and best practices for drug discovery. *J. Chem. Inf. Model.*, **60**, 5595–5623.
79. Maier,J.A., Martinez,C., Kasavajhala,K., Wickstrom,L., Hauser,K.E. and Simmerling,C. (2015) ff14SB: improving the accuracy of protein side chain and backbone parameters from ff99SB. *J. Chem. Theory Comput.*, **11**, 3696–3713.
80. Tendwa,M.B., Chebon-bore,L., Lobb,K., Musyoka,T.M. and Tastan Bishop,Ö. (2021) Force field parameters for fe2+ 4s2−4 clusters of dihydropyrimidine dehydrogenase, the 5-fluorouracil cancer drug deactivation protein: a step towards in silico pharmacogenomics studies. *Molecules*, **26**, 2929.
81. Bourgeois,G., Seguin,J., Babin,M., Gondry,M., Mechulam,Y. and Schmitt,E. (2020) Structural basis of the interaction between cyclodipeptide synthases and aminoacylated tRNA substrates. *Rna*, **26**, 1589–1602.
82. Pérez,A., Marchán,I., Svozil,D., Sponer,J., Cheatham,T.E., Laughton,C.A. and Orozco,M. (2007) Refinement of the AMBER force field for nucleic acids: Improving the description of α/γ conformers. *Biophys. J.*, **92**, 3817–3829.
83. Zgarbová,M., Otyepka,M., Šponer,J., Mládek,A., Banáš,P., Cheatham,T.E. and Jurečka,P. (2011) Refinement of the Cornell et al. Nucleic acids force field based on reference quantum chemical calculations of glycosidic torsion profiles. *J. Chem. Theory Comput.*, **7**, 2886–2902.
84. Aduri,R., Psciuk,B.T., Saro,P., Taniga,H., Schlegel,H.B. and SantaLucia,J. (2007) AMBER force field parameters for the naturally occurring modified nucleosides in RNA. *J. Chem. Theory Comput.*, **3**, 1464–1475.
85. Yan,Y., Tao,H., He,J. and Huang,S.Y. (2020) The HDOCK server for integrated protein–protein docking. *Nat. Protoc.*, **15**, 1829–1852.
86. Paysan-Lafosse,T., Blum,M., Chuguransky,S., Grego,T., Pinto,B.L., Salazar,G.A., Bileschi,M.L., Bork,P., Bridge,A., Colwell,L., *et al.* (2023) InterPro in 2022. *Nucleic Acids Res.*, **51**, D418–D427.
87. Benson,D.A., Cavanaugh,M., Clark,K., Karsch-Mizrachi,I., Lipman,D.J., Ostell,J. and Sayers,E.W. (2017) GenBank. *Nucleic Acids Res.*, **45**, D37–D42.
88. Echarren,M.L., Figueroa,N.R., Vitor-Horen,L., Pucciarelli,M.G., García-del Portillo,F. and Soncini,F.C. (2021) Balance between bacterial extracellular matrix production and intramacrophage proliferation by a Salmonella-specific SPI-2-encoded transcription factor. *Mol. Microbiol.*, **116**, 1022–1032.
89. Tremblay,B.J.M., Lobb,B. and Doxey,A.C. (2021) PhyloCorrelate: inferring bacterial gene-gene functional associations through large-scale phylogenetic profiling. *Bioinformatics*, **37**, 17–22.
90. Cho,G., Lee,J. and Kim,J. (2023) Identification of a novel 5-aminomethyl-2-thiouridine methyltransferase in tRNA modification. *Nucleic Acids Res.*, **51**, 1971–1983.
91. Endres,L., Dedon,P.C. and Begley,T.J. (2015) Codon-biased translation can be regulated by wobble-base tRNA modification systems during cellular stress responses. *RNA Biol.*, **12**, 603–614.
92. Hori,H., Kawamura,T., Awai,T., Ochi,A., Yamagami,R., Tomikawa,C. and Hirata,A. (2018) Transfer RNA modification enzymes from thermophiles and their modified nucleosides in tRNA. *Microorganisms*, **6**, 110.
93. Lu,Z. and Imlay,J.A. (2019) A conserved motif liganding the [4Fe–4S] cluster in [4Fe–4S] fumarases prevents irreversible inactivation of the enzyme during hydrogen peroxide stress. *Redox Biol.*, **26**, 101296.

94. Hoang,C. and Ferré-D'Amaré,A.R. (2001) Cocrystal structure of a tRNA Ψ55 pseudouridine synthase: Nucleotide flipping by an RNA-modifying enzyme. *Cell*, **107**, 929–939.
95. Söding,J., Biegert,A. and Lupas,A.N. (2005) The HHpred interactive server for protein homology detection and structure prediction. *Nucleic Acids Res.*, **33**, 244–248.
96. Holm,L., Kääriäinen,S., Rosenström,P. and Schenkel,A. (2008) Searching protein structure databases with DaliLite v.3. *Bioinformatics*, **24**, 2780–2781.
97. Favre,A., Hajnsdorf,E., Thiam,K. and Caldeira de Araujo,A. (1985) Mutagenesis and growth delay induced in Escherichia coli by near-ultraviolet radiations. *Biochimie*, **67**, 335–342.
98. Oppezzo,O.J. and Pizarro,R.A. (2001) Sublethal effects of ultraviolet A radiation on Enterobacter cloacae. *J. Photochem. Photobiol. B Biol.*, **62**, 158–165.
99. Takano,H., Agari,Y., Hagiwara,K., Watanabe,R., Yamazaki,R., Beppu,T., Shinkai,A. and Ueda,K. (2014) LdrP, a cAMP receptor protein/FNR family transcriptional regulator, serves as a positive regulator for the light-inducible gene cluster in the megaplasmid of Thermus thermophilus. *Microbiol. (United Kingdom)*, **160**, 2650–2660.
100. Sumi,S., Mutaguchi,N., Ebuchi,T., Tsuchida,H., Yamamoto,T., Suzuki,M., Natsuka,C., Shiratori-Takano,H., Shintani,M., Nojiri,H., *et al.* (2020) Light response of Pseudomonas putida KT2440 mediated by class II LitR, a photosensor homolog. *J. Bacteriol.*, **202**, e00146-20.
101. Maruyama,T., Sumi,S., Kobayashi,M., Ebuchi,T., Kanesaki,Y., Yoshikawa,H., Ueda,K. and Takano,H. (2022) Class II LitR serves as an effector of "short" LOV-type blue-light photoreceptor in Pseudomonas mendocina. *Sci. Rep.*, **12**, 21765.
102. Blanchetot,A., Hajnsdorf,E. and Favre,A. (1984) Metabolism of tRNA in near-ultraviolet-illuminated Escherichia coli The tRNA repair hypothesis. *Eur. J. Biochem.*, **139**, 547–552.
103. Brown,A., Fernández,I.S., Gordiyenko,Y. and Ramakrishnan,V. (2016) Ribosome-dependent activation of stringent control. *Nature*, **534**, 277–280.
104. Kramer,G.F., Baker,J.C. and Ames,B.N. (1988) Near-UV stress in Salmonella typhimurium: 4-Thiouridine in tRNA, ppGpp, and ApppGpp as components of an adaptive response. *J. Bacteriol.*, **170**, 2344–2351.
105. Probst-Rüd,S., McNeill,K. and Ackermann,M. (2017) Thiouridine residues in tRNAs are responsible for a synergistic effect of UVA and UVB light in photoinactivation of Escherichia coli. *Environ. Microbiol.*, **19**, 434–442.
106. Probst-Rüd,S., Nyangaresi,P.O., Adeyeye,A.A., Ackermann,M., Beck,S.E. and McNeill,K. (2024) Synergistic effect of UV-A and UV-C light is traced to UV-induced damage of the transfer RNA. *Water Res.*, **252**, 121189.
107. Tulin,G., Figueroa,N.R., Checa,S.K. and Soncini,F.C. (2024) The multifarious MerR family of transcriptional regulators. *Mol. Microbiol.*, **121**, 230–242.
108. Oppezzo,O.J. and Pizarro,R.A. (2002) Transient reduction in the tRNA 4-thiouridine content induced by ultraviolet A during post-irradiation growth in Enterobacter cloacae. *J. Photochem. Photobiol. B Biol.*, **66**, 207–212.

Received: May 13, 2024. **Revised:** July 30, 2024. **Editorial Decision:** August 1, 2024. **Accepted:** August 7, 2024